Article:

Prescott, C, Haywood, A orcid.org/0000-0001-7008-0534, Dolan, A et al. (2 more authors) (2019) Indian monsoon variability in response to orbital forcing during the late Pliocene. Global and Planetary Change, 173. pp. 33-46. ISSN 0921-8181

https://doi.org/10.1016/j.gloplacha.2018.12.002

INDIAN MONSOON VARIABILITY IN RESPONSE TO ORBITAL FORCING DURING THE LATE PLIOCENE

[1]*Prescott, C.L., [1]Haywood, A.M., [1]Dolan, A.M., [1]Hunter, S.J. and [1]Tindall, J.C.

[1]School of Earth and Environment, University of Leeds, Woodhouse Lane, Leeds, UK, LS2 9JT

*Corresponding author: C.L. Prescott (js07c2lp@leeds.ac.uk).

Abstract

The Asian monsoon is a major component of the global climate system and can be divided into two subsystems, the Indian monsoon and the East Asian monsoon. Insights into monsoon behaviour and dynamics can be gained through studying past warm intervals in Earth's history. One such interval is the Pliocene epoch, specifically the mid-Piacenzian Warm Period (mPWP; 3.264 – 3.025 Ma). This time is characterised as a period of sustained warmth, with annual mean temperatures 2 to 3°C higher than the pre-industrial era. Studies have examined the East Asian monsoon during the mPWP from both a geological data and climate modelling perspective. However, there has been little investigation into the behaviour of the Indian monsoon. Using a coupled atmosphere-ocean global climate model (HadCM3), the Indian summer monsoon response to orbital forcing during the mPWP is studied.

Of the simulated interglacial events (Marine Isotope Stages KM5c, KM3, K1 and G17), MIS KM5c is the only one with a near-modern orbital forcing. This experiment is compared to a pre-industrial simulation to determine the nature of the mPWP Indian summer monsoon in the absence of a different pattern if insolation forcing. The monsoon at MIS KM5c, is simulated to be stronger than pre-industrial, with higher surface air temperatures and precipitation over land due to higher levels of CO_2. MIS G17, K1, and KM3 represent interglacial events of similar magnitude with different insolation forcing than MIS KM5c. The Indian summer monsoon is simulated to be significantly stronger for the interglacials K1 and KM3, compared to KM5c. This is due to stronger precession forcing causing an increase in summer surface air temperature and precipitation. When combined with Pliocene geological boundary conditions, these results highlight the significant effect of orbital forcing on the strength of the Indian summer monsoon. The sensitivity of the Indian monsoon to orbital forcing has important implications for any parallels drawn between Pliocene and future monsoon behaviour.

1. Introduction

1.1 The Asian monsoon and the Pliocene

The Intergovernmental Panel on Climate Change (IPCC) defines monsoons as a seasonal phenomenon responsible for producing the majority of wet-season rainfall within the tropics (Christensen et al., 2013). Monsoon circulation is driven by the difference in temperature between land and sea, which varies seasonally with the distribution of solar heating (Christensen et al., 2013). The duration and amount of rainfall depends on the moisture content of the air and on the configuration and strength of atmospheric circulation (Christensen et al., 2013). The Asian monsoon represents a major component of the global climate system and influences societal and economic activity for almost two thirds of the world's population (Webster et al., 1998; Ao et al., 2016). The strength and variability of the Asian monsoon has been, and continues to be, crucial to the prosperity of the region (Clift and Plumb, 2008). The Asian monsoon includes at least two subsystems: The Indian monsoon (or South Asian monsoon) and the East Asian monsoon roughly divided at ~105°E (Wang et al., 2005). The two systems are linked and respond to the strength of the continental high and low-pressure cells. However, they also have significant differences due to different land-sea distributions (Wang et al., 2005).

Valuable insights into future monsoon behaviour may be gained by investigating monsoon behaviour during past warm intervals. One of these past warm intervals is the Pliocene epoch (5.33-2.58 Ma). The Pliocene maybe particularly useful for understanding future climate dynamics due to similar continental configurations, land elevations and ocean bathymetries to the present day (Haywood et al., 2016) and warming being related, at least in part to CO_2 forcing. The mPWP is characterised as a period of sustained warmth in Earth's history with annual mean temperatures thought to be 2-3°C higher than pre-industrial (Haywood & Valdes, 2004; Haywood et al., 2013). A considerable effort has been made to understand the climate of the mPWP through a combination of modelling and geological data reconstruction.

There are a number of studies of the East Asian monsoon behaviour in the Pliocene from both a data and modelling perspective. Published work on the Chinese Loess Plateau indicates an enhanced East Asian Summer Monsoon (EASM) during the Piacenzian Stage (Ding et al., 2001; Ao et al., 2016), and a relatively weak East Asian Winter Monsoon (EAWM; Chen et al., 2006; Wang et al., 2007). Yan et al. (2012) found a stronger than present EASM using the Community Atmosphere Model version 3.1 (CAM3.1) but could not reproduce the weakened EAWM seen in the proxy data. A multi-model comparison of the East Asian monsoon from the Pliocene Model Intercomparison Project (PlioMIP) (Zhang et al., 2013) found that East Asian Summer Winds largely strengthen in monsoonal China which qualitatively agrees with geological reconstructions, a discrepancy between the different models was noted when simulating the East Asian Winter Winds. However, six models simulated a weakened mid-Pliocene East Asian winter winds and nine models more intense (Zhang et al., 2013). The weakened East Asian winter winds were caused by larger decreases in the sea-level pressure gradient in the boreal winter due to stronger winter warming over China than the multi-model mean. These different responses to the same radiative forcing in the PlioMIP ensemble are speculated to be related to independent changes in boundary conditions (e.g. land-cover/vegetation) and/or physical processes and parameterisation in the models (Zhang et al., 2013).

1.2 Indian Monsoon

There has been less investigation into the behaviour of the Indian monsoon in the Pliocene and this study focuses on that sub-system of the Asian monsoon (Fig. 1). The present day Indian monsoon is driven by large seasonal variations in wind direction over the Indian subcontinent and surrounding oceans (Gadgil et al., 2003). Due to the seasonal cycle of solar heating during boreal spring, the south Asian landmass is warmed faster than the ocean, owing to differences in heat capacity (Turner & Annamalai, 2012). This results in the formation of a surface heat low over northern India and winds are driven from the southwest to northeast towards the continent. In contrast in winter (November to February), the pressure cells reverse and winds flow from northeast to southwest (Gupta & Anderson, 2005). This pattern of seasonally reversing winds transports moisture from over the warm Indian Ocean and ultimately contributes 80% of annual rainfall to south Asia between June and September (Turner & Annamalai, 2012). In contrast, during winter the dry continental air blows from the northeast which results in very low rainfall.

1.2.1 The Pliocene Indian Monsoon

Due to limited availability of high temporal resolution marine sediments and few terrestrial records describing the history of the Indian monsoon variability, the nature of Indian monsoon variability in the Pliocene remains largely unknown. A terrestrial sedimentary sequence from the Yanmou Basin in Southwest China, where the climate is thought to be controlled by the Indian monsoon in summer bringing rainfall from the tropical Indian Ocean to the Basin, was presented by Chang et al. (2010). A general trend of increased clay and clay plus fine silt fractions accompanied by an increase in sedimentation rate was found. This suggested a gradual intensification of the Indian summer monsoon from 3.57 to 2.78 Ma. A terrestrial study using the leaf physiognomic spectrum examined the late

Pliocene Longmen flora on the eastern side of Mt Gaoligong and Mt Nu in western Yunnan (Western China) (Su et al., 2013). The results indicated that the Asian monsoon during the late Pliocene was not as strong as present day in western Yunnan. There was however, an amplification from the late Miocene to the late Pliocene (Su et al., 2013). However, since the western Yunnan experiences both the East Asian monsoon and the Indian monsoon (Wang, 2006) this study could not robustly distinguish the two.

Sediments deposited in the Himalayas foreland of early Miocene to Pliocene age are known as the Siwalik group. Carbon and oxygen isotope ratios of soil carbonate nodules, and carbon isotope ratio of associated organic matter, were measured from three Indian Siwalik successions. Variations in soil carbonate $\delta^{18}O$ suggest a clear onset of the monsoon system at 6 Ma, with a peak of intensity at 5.5 Ma, followed by a gradual decrease in monsoon strength until it attained modern-like conditions with minor fluctuations (Sanyal et al., 2004).

Mohan and Gupta (2011) analysed a 5.6-million-year proxy record of surface dwelling planktic foraminifera from Deep Sea Drilling Project Site 219. They suggest that the monsoon regime over Site 219 in the southeast Arabian Sea switched between summer (southwest) and winter (northeast) monsoons on glacial-interglacial timescales, with more influence of the summer monsoon during warm periods and the winter monsoon during cold periods. A major shift in the physical character of the surface ocean in the southeast Arabian Sea was observed at ~3.4 Ma, indicating a change in monsoon wind intensities, and a switch to surface productivity being driven by winter monsoon winds linked to the expansion of the Northern Hemisphere glaciation (Mohan & Gupta, 2011). Gupta and Thomas (2003) found an important change in monsoon behaviour between 3.2 and 2.5 Ma in their analysis of benthic foraminifera from Site 758 in the northern Indian Ocean. They found indications of high seasonality, demonstrated by a faunal change between 3.2 and 2.5 Ma consisting of a change from overall high-productivity, non-opportunistic species-dominated biofacies, to biofacies dominated by opportunist species (Gupta & Thomas, 2003).

In a multi-proxy organic geochemical record from Deep Sea Drilling Project Site 231 in the Gulf of Aden spanning 5.3 – 2 Ma, warm subsurface ocean temperatures were found in the earliest Pliocene with ocean temperatures cooling after 5 Ma (Liddy et al., 2016). A transition to arid conditions on land was found at 4.3 Ma appearing to be due to an atmospheric response to cooling ocean temperatures. The authors suggest this may reflect changes in tropical ocean circulation or the intensification of Indian Monsoon winds (Liddy et al., 2016). Another multiproxy study of a sediment core from Ocean Drilling Program (ODP) Site 722 in the Arabian Sea found an alkenone sea surface temperature (SST) record with similar trends to the global benthic foraminifera $\delta^{18}O$ record over the past 11 Ma showing low amplitude variations from 11 to 5 Ma, a slight decrease in temperature from 5 to 4 Ma, followed by high amplitude variability from 4 to 0.7 Ma (Huang et al., 2007).

Given the ambiguity or lack of consistency of proxy-based interpretations listed above, the nature of the Indian monsoon and its variability during the Pliocene is unclear and can be interpreted several ways. Overall the proxy reconstructions indicate high variability in the Indian monsoon throughout the Pliocene with some proxies suggesting an intensification from the Miocene while others indicate a decrease in strength.

In the first climate modelling study of the Indian monsoon during the Pliocene, the atmosphere only Community Atmosphere Model version 4 (CAM4) was used to investigate the effects of different PRISM3 boundary conditions on the simulation of the summer monsoon (Zhang & Zhang, 2017). The impact of altered mid-Piacenzian topography, land cover and combined CO_2 and SSTs were compared to each other and to a pre-industrial simulation. The study found the combined CO_2 concentration (405ppm), and PRISM3 SSTs, to be the most important factor responsible for simulating the largest difference between the mid-Piacenzian and pre-industrial summer monsoons (Zhang & Zhang, 2017). In comparison, the changes in vegetation and topography had a limited effect on the intensification of the Indian monsoon (Zhang & Zhang, 2017). The simulations analysed in this study all had a modern orbit and, in the concluding, remarks the authors suggest that further investigation into the effect of orbital forcing on the predicted monsoon is necessary.

1.2.2 The effect of orbital forcing on the Indian monsoon

There is a wide range of evidence from different environmental indicators over land, ice and ocean that the Asian monsoon varies depending on insolation (Wang et al., 2005; Braconnot et al., 2008), and that orbital forcing has affected the long term evolution of the Asian monsoon (Liu & Shi, 2009). Variations in the Earth's orbit cause shifts in the distribution of incoming solar radiation to Earth (Hays et al., 1976; Berger, 1978). Precession, obliquity and eccentricity are three parameters of the earth's orbit controlling this distribution of solar radiation at the top of the atmosphere (Liu & Shi, 2009). Precession controls the amount of insolation that reaches Earth specifically as a function of seasons (Overpeck et al., 1996). It is the key parameter that determines at which time in the year maximum or minimum insolation occurs, as well as length of the seasons (Berger, 1988). Summer insolation is largest for periods where the Earth is near the perihelion of its orbit in summer. The resulting continental heating over the Northern Hemisphere cause an intensification of monsoon flow

(Prell & Kutzbach, 1987). There is a clear link between orbital forcing, specifically the precession cycle and the strength of monsoons (Clemens & Prell, 1990; Braconnot & Marti, 2003). Changes in climate boundary conditions, such as ice volume, snow cover in the Himalayas, sea surface temperatures (SSTs), albedo, and atmospheric gas concentrations, modulate the response of the monsoon to solar insolation (Prell & Kutzbach, 1992; deMenocal & Rind, 1993; Overpeck et al., 1996). It is therefore an oversimplification to assume that all summer monsoons during interglacials are strong in the same way that not all summer monsoons during glacial times are weak (Prell & Kutzbach, 1992).

In general, efforts in modelling and reconstructing the Piacenzian stage (including the PlioMIP project) have predominantly focused on reconstructing an average Pliocene climate. This includes Pliocene modelling studies looking at the behaviour of monsoon systems (such as Zhang et al., 2013). Recently however, efforts have been made to try to understand how the climate varies, even within this ‘stable’ warm period. In Prescott et al. (2014) large seasonal temperature differences were seen between simulations of two interglacials with different orbital forcings. Building on this, the monsoonal variation within the Piacenzian Stage was investigated by simulating and comparing the Indian monsoon in four Late Pliocene Interglacial time slices with different orbits. An aspect of this study that differs from the majority of current Pliocene literature is that instead of analysing idealised orbital forcing experiments or hypothetical scenarios, actual orbital forcing parameters corresponding to the four largest interglacial peaks seen in the LR04 benthic oxygen isotope stack (Lisiecki & Raymo, 2005) within the Piacenzian stage have been used. While it might be expected that interglacial periods would display strong monsoons, as has been shown in the Quaternary (Prell & Campo, 1986), the orbital forcing study of Prescott et al. (2014) found that interglacials within the Piacenzian stage vary in magnitude. More specifically, a recent vegetation modelling study looking at the same four largest interglacial peaks (Prescott et al., 2018) found particularly large seasonal changes in surface air temperatures (SAT) and vegetation over the Asian continent.

The four Pliocene interglacials are simulated using the Met Office Hadley Centre Global Coupled model, HadCM3; Marine Isotope Stages (MIS) KM5c (3.205 Ma), KM3 (3.155 Ma), K1 (3.060 Ma) and G17 (2.950 Ma) (Fig. 2). These are the four most negative benthic oxygen isotope excursions seen in the LR04 benthic oxygen isotope stack (Lisiecki & Raymo, 2005) during the Piacenzian Stage. The specific orbit used in the simulations represents the peak of each interglacial event. Haywood et al. (2013) show that the peak of MIS KM5c is characterised by a near modern orbital forcing within a period of low eccentricity and low precession (Laskar et al., 2004; Prescott et al., 2014). In this study, therefore, when examining changes in the climatology in the simulations of the four interglacials, KM5c is considered as the control Pliocene experiment. Here, the Indian monsoon in KM5c is compared to the pre-industrial and then KM5c is compared to the other three interglacials (G17, K1, and KM3) that display a different pattern of orbital forcing.

1.3 Specific research questions:

1) How does HadCM3 simulate the Indian Monsoon in the Pliocene for MIS KM5c (an interglacial with a near modern orbit) compared to the pre-industrial era?
2) How does the simulation of the Indian monsoon change when simulating three further Pliocene interglacials with orbital forcing substantially different to modern?
3) What does the modelled variability in the Indian monsoon behaviour imply about interpreting discrete and often time specific proxy records of Indian monsoon behaviour?

2. Methods

2.1 The climate model

The simulations were all carried out using HadCM3. HadCM3 is a dynamically and thermodynamically coupled atmosphere, ocean and sea ice model. The resolution of the atmosphere is 2.5° in latitude by 3.75° in longitude and contains 19 layers with a time step of 30 minutes. The ocean model has a resolution of 1.25 by 1.25 with 20 layers. A full description of the model can be found in Gordon et al. (2000), Cox et al. (1999) and Valdes et al. (2017). HadCM3 has been widely used for palaeoclimate modelling, with simulations of the Last Glacial Maximum and Mid-Holocene climates as well as the mPWP and deeper time. The model represents the seasonal cycle of the Indian monsoon well for the modern compared to other similarly complex models. (Turner et al., 2007). The experiments were run for 500 years with the final 100 years used to calculate the required climatological averages.

In this version of HadCM3, the Met Office Surface Exchange Scheme version 2.1 (MOSES2.1) was used coupled to a dynamic vegetation model (Top-down Representation of Interactive Foliage and Flora Including Dynamics; TRIFFID). TRIFFID computes the structure and distribution of six plant functional types and can be run in both equilibrium and dynamic mode. The equilibrium mode is coupled asynchronously to the atmosphere model, with accumulated carbon fluxes passing through MOSES2.1 (Cox 2001). The experiments were run using equilibrium mode for the first 50 years and then run with dynamic mode for the remainder of the simulation. Previous modelling studies have demonstrated that the inclusion of dynamic vegetation could contribute to the enhancement of the orbitally-induced monsoon change for both the Holocene and modern (Li et al., 2009). Similarly, Braconnot et al. (1999) determined the importance of including vegetation feedbacks in simulations of the African monsoon, yielding model results in better agreement with observations.

2.2 Boundary conditions

Results are presented from five climate model simulations (Table 1.). Four experiments were run with HadCM3 based on the experimental design from the PlioMIP project (Haywood et al., 2010; Bragg et al., 2012), that used PRISM3D boundary conditions (Dowsett et al., 2010) but with the addition of dynamic vegetation and the MOSES2.1 land surface scheme. An experiment with pre-industrial boundary conditions was also run for comparison purposes. As in the PlioMIP project the Pliocene experiments CO_2 concentration is set to 405 ppmv, with other trace gases and aerosols consistent at pre-industrial levels. The PRISM3D ice sheet reconstruction includes a much reduced Greenland ice sheet with East Antarctica showing little change and significant retreat in the Wilkes and Aurora sub-glacial basins compared to modern (Haywood et al., 2010). The PRISM3D topographic reconstruction was used to provide palaeogeographic boundary conditions (Sohl et al., 2009). This is quite similar to modern apart from the coastline adjusted for the 25m higher than modern sea level, the Hudson Bay filled to low elevation and an absent West Antarctic ice. Most relevant to this study, the elevations for the Tibetan Plateau were made roughly consistent with modern day due to uncertainty over the timing of plateau uplift (Sohl et al., 2009).

2.3 Orbital Forcing

While the PlioMIP project specified a modern orbital configuration, here simulations for Marine Isotope Stages (MIS) G17, K1, KM3 and KM5c have been performed using orbital parameters derived from the Laskar et al. (2004) astronomical solution. In order to take into account the changes in the length of the seasons determined by variations in the date of perihelion along a precession cycle, a calendar correction from the modern day calendar is applied, as discussed in Marzocchi et al. (2015) using the method documented in Pollard & Reusch (2002). This conversion method estimates angular monthly calendar means from mean model output on a modern calendar, therefore reducing incorrect calendar effects (Pollard & Reusch, 2002). A modification is included from the Pollard and Reush (2002) method, detailed in Marzocchi et al. (2015), to take the 360-day model year simulated in HadCM3 into account.

2.4 Monsoon Indices

To compare the five experiments beyond their climatological patterns, monsoon indices have been calculated (Table 1). The Extended Indian Monsoon Rainfall (EIMR) index, rather than solely looking at rainfall over the Indian subcontinent, includes precipitation over the neighbouring land and seas as affected by the Indian monsoon (Goswami et al., 1999). The EIMR index is the average precipitation per day over the area 70°E - 110°E, 10°N - 30°N (shown by the shaded area in Fig. 1). As well as the precipitation-based index, Goswami et al. (1999) proposed that the Hadley circulation represents the strength of the Indian summer monsoon circulation. The shear of meridional wind between the lower and upper troposphere (between 850 and 200 hPa) was found to be a good measure of the Hadley circulation averaged over the same region as the EIMR index (70°E - 110°E, 10°N - 30°N), therefore the Monsoon Hadley Index (MHI) is also used here:

$$MHI = V_{850} - V_{200}$$

Where V_{850} and V_{200} are the meridional wind anomalies at 850 hPa and 200 hPa averaged over the summer months (June – September) and over the monsoon region (70°E - 110°E, 10°N - 30°N) (Goswami et al., 1999).

3. Results

3.1 Comparing the KM5c and pre-industrial simulation

The simulated climate over the Indian monsoon region during summer (JJAS) for KM5c and pre-industrial share similar patterns in predicted climate variables albeit with different intensities (Fig. 3). The simulated seasonal surface air temperature (SAT) for KM5c is higher for both land and ocean than pre-industrial (Fig. 3a). Simulated temperatures reached 43.7°C in KM5c and 43.0°C in pre-industrial over northwest India and 49.1°C in KM5c and 45.5°C in pre-industrial over the Middle East (Fig. 3a). When looking at the SAT difference between KM5c and pre-industrial there are individual grid boxes showing SAT differences of up to 8°C higher in KM5c than the pre-industrial (Fig. 3a). The highest SATs are predominantly seen north of 30°N in KM5c, when compared to pre-industrial, whereas there are similar temperatures over India (31.0°C in KM5c compared to 29.6°C in pre-industrial) with some areas to the northwest of India simulating cooler temperatures than pre-industrial (up to ~4°C) (Fig. 3a).

For both KM5c and pre-industrial the highest precipitation occurs in the South China Sea (reaching a maximum of 26.4 mm/day in KM5c and 22.9 mm/day in pre-industrial) and the Bay of Bengal (18.8 mm/day in KM5c and 15.6 mm/day in pre-industrial) (Fig. 3b). There is also a band of high rainfall between 2 – 10°N across the Indian Ocean (Fig. 3b). A similar pattern of precipitation over terrestrial areas is predicted in both experiments with high rainfall over most of South and South-East Asia, on average 10.3 mm/day for pre-industrial and 10.8 mm/day for KM5c (Fig. 3b). For KM5c however, the model simulates more precipitation (up to ~5 mm/day) across India, into Southern China and the northern Bay of Bengal with further increases in the Indian Ocean. The simulated precipitation in KM5c is on average 2.0 mm/day less than pre-industrial across Thailand, Cambodia and into the South China Sea (Fig. 3b). The precipitation differences between the two experiments is driven by differences in convective rainfall (Suppl Fig. 3d).

The lowest mean sea level pressure (MSLP) in summer occurs over the high topographic area of western China (between 30 – 35°N) for the KM5c (985 hPa) and the pre-industrial (990 hPa), with surrounding areas characterised by higher pressure (on average 1011 hPa over Indian Ocean in pre-industrial with KM5c simulating 1008 hPa for the same area) (Fig. 3c). KM5c has lower mean sea level pressure than pre-industrial throughout the whole monsoon area with the largest difference between 32°N and 45°N over continental Asia where the pressure is on average 6.4 hPa lower than the pre-industrial simulation. Whereas between 5°S and 5°N over the Indian Ocean the simulated MSLP for KM5c is only 3.0 hPa lower than the pre-industrial simulation (Fig. 3c).

Both KM5c and the pre-industrial simulate the same pattern of surface winds blowing inland from the equatorial Indian Ocean, across the Horn of Africa and into continental Asia blowing eastwards across the Arabian Sea into India and across the Bay of Bengal (Fig. 3c). In KM5c the winds are simulated to be weaker than those simulated in the pre-industrial across India and Bay of Bengal but stronger across the Horn of Africa and the Arabian Sea (Fig. 3c) following a pattern of decreased pressure in this area in KM5c compared to pre-industrial.

The sea surface temperatures (SSTs) are ~2°C higher in KM5c than pre-industrial with the temperature increase mainly focussed in the Indian Ocean and Bay of Bengal (Fig. 3e). Both KM5c and pre-industrial are most saline in the Arabian Sea and Western Indian Ocean (both approximately 37 PSU) and least saline in the Yellow Sea and the South East Asian Seas (KM5c on average 26.3 PSU and pre-industrial 27.6 PSU) (Suppl. Fig. 3b). The salinity simulated in KM5c is very similar to pre-industrial throughout the monsoon area, apart from in the Yellow Sea which is up to 5 PSUs less saline (Suppl. Fig. 4b). The simulated runoff for both KM5c and pre-industrial predicts high runoff in areas with the highest simulated precipitation, Southern China, Northeast India and South-East Asia (Suppl. Fig. 3c). For KM5c the model simulates on average 4.7 mm/day over these areas (on average 1.8 mm/day more than pre-industrial) and reaches a maximum of 11mm/day (Suppl. Fig. 2c and 3c). High percentage cloud cover is simulated over south and south-east Asia (on average ~80%) for both KM5c and pre-industrial with little cloud simulated to western Asia and western Indian Ocean, approximately 24% for both (Fig. 3d). The model simulates more cloud cover over India (6% more) for KM5c but in general simulates minimal differences from the pre-industrial simulation (Fig. 3d).

3.2 Comparing G17, K1 and KM3 with the KM5c control

Superficially the patterns of summer SAT are very similar between all simulated interglacials as seen in the figures of absolute model results (Fig. 4). There are however some changes in temperature between KM5c and the other three interglacials. G17, K1 and KM3 simulate higher temperatures over continental Asia than KM5c (average increases of 2.9°C in G17, 6.6°C in K1 and 5.9°C in KM3), especially over west Asia/Middle East and 35°N and above over the rest of Asia (Fig. 4). The largest predicted temperature differences are simulated in K1 and KM3 compared to KM5c with a maximum SAT change of 9.3°C in K1 and 10.4°C in KM3 over Asia (Fig. 4). The model simulates some warming for all three interglacials over the ocean compared to KM5c, on average 1.2°C warmer in G17, 2.2°C warmer in K1 and 2.0°C warmer in KM3 (averaged over 10°S to 5°N) (Fig. 4). Whereas, for all three interglacials the SATs predicted over latitudes 20°N to 30°N show little change from the KM5c control (Fig. 4). There are also areas showing simulated cooling compared to KM5c. The north west of India (maximum decrease of 4.7°C in G17, 5.3°C in K1 and 7.1°C in KM3) the southern tip of India (increase of 0.3°C in G17 but up to 4.9°C cooler in K1 and 4.4°C in KM3), and Oman and Yemen (maximum decrease of 4.4°C in G17, 5.3°C in K1 and 6.3°C in KM3) (Fig. 4).

The model predicts lower MSLP than in KM5c for all three interglacials from 25°N and above, with average decreases of 1.9 hPa in G17, 5.2 hPa in K1 and 4.5 hPa in KM3 (Fig. 5). Slightly lower pressure than KM5c is also predicted over the Indian Ocean (10°S to 5°N), 0.5 hPa in G17, 0.8 hPa in K1 and 0.9 hPa in KM3 (Fig. 5). There is, however, an area of higher pressure compared to KM5c reaching 5.6 hPa in G17, 7.1 hPa in K1 and 7.0 hPa in KM3 (Fig. 5). This area of higher pressure is largest between 25°N and 40°N in the West Pacific Ocean and extends latitudinally across eastern Asia to northern India. There is lower pressure than KM5c across the Middle East but higher pressure across northern and eastern India (Fig. 5). Due to this, there is a decrease in surface wind strength moving from the Arabian Sea into the Indian subcontinent in the interglacials compared to KM5c in addition to the weaker winds that flow across the Bay of Bengal into East Asia (Fig. 5). The lower pressure compared to KM5c over the Middle East results in increased wind strength from the Gulf of Aden into Yemen, Oman and Saudi Arabia (Fig. 5).

The precipitation changes simulated between the three interglacials and KM5c show greater differences than between the Pliocene KM5c control and pre-industrial simulation (Fig. 6). In contrast to the SAT results (Fig. 4), the largest increases in summer precipitation compared to KM5c are seen across northern India and between 20°N and 30°N across the south Asian terrestrial areas reaching maximum increases of 4.3 mm/day in G17, 13.0 mm/day in K1 and 11.4 mm/day in KM3 (Fig. 6). The area over India (the All Indian Rainfall (AIR) Lat 7-30°N, Lon 65 - 95°E) simulates on average increases from KM5c of 1.0 mm/day in G17, 2.9 mm/day in K1 and 2.4 mm/day in KM3 (Fig. 6). With some decreases in precipitation over the Bay of Bengal (approximately 0.8 mm/day less than KM5c in K1 and KM3) and the East and South China Seas (decrease from KM5c of up to 5.2 mm/day in G17, 8.7 mm/day in K1 and 9.0 mm/day in KM3) and to the east of equatorial Indian Ocean (Fig. 6). There are also increases of up to 3.5 mm/day in G17, 4.4 mm/day in K1 and 5.3 mm/day in KM3 in the northern Indian Ocean (Fig. 6).

The increases in precipitation compared to KM5c are driven by a combination of convective rainfall and largescale rainfall, with the changes in largescale rainfall mainly driving the increased band of precipitation across northern India and the decreases of precipitation over oceanic areas due to less convective rainfall in these areas (Suppl. Fig. 4d and 4e). The increased precipitation across terrestrial southern Asia is strongly matched by increases in runoff throughout northern India and across China reaching the eastern coast in all three interglacials predicting average runoff increases from KM5c of 1.5 mm/day in G17, 4.0 mm/day in K1 and 3.7 mm/day in KM3 (Suppl. Fig. 4c). These increases in precipitation and runoff cause localised decreases in salinity just off the coast of the Bay of Bengal and Arabian Sea of up to 4.5 PSUs in G17, 8.9 PSUs in K1 and 8.5 PSUs in KM3 less than KM5c (Suppl. Fig. 4b). There is also decreased salinity of on average 0.9 PSU in G17, 3.0 PSU in K1 and 2.2 PSU in the Indian Ocean (largest between 3°N and 6°N) (Suppl. Fig. 4b). Increases in salinity are observed in the south Asian seas, on average 0.6 PSUs in G17, 1.7 PSUs in K1 and 1.5 PSUs in KM3 more than KM5c, in the areas where a decrease of precipitation is seen (Fig. 6 and Suppl. Fig. 4b. The interglacials all show increased cloud cover compared to KM5c over terrestrial areas, reaching increases of 19% in G17, 33% in K1 and 32% in KM3 over Northern India and the Middle East, with increases in the Arabian Sea and western Indian Ocean (increases of 28% in K1 and 24% in KM3 compared to KM5c) (Fig. 7). There is also a decrease in cloud cover in the south-East Asia region in the interglacials compared to KM5c (Fig. 7).

Higher SSTs are observed in the three interglacials compared to KM5c (Fig. 8). This increase of SSTs is on average 1°C in G17, 1.4°C in K1 and 1.5°C in KM3 higher than KM5c over the Indian Ocean between 10°S and 5°N (Fig. 8). There are larger difference in SSTs over the Arabian Sea with the interglacials reaching up to 2.2°C in G17, 2.8°C in K1 and 2.4°C in KM3 higher than KM5c (Fig. 8).

4. Discussion

4.1 How does HadCM3 simulate the Indian Monsoon in the Pliocene for MIS KM5c (an interglacial with a near modern orbit) compared to the pre-industrial era?

Rather than just looking at the rainfall over the Indian subcontinent, the Extended Indian Monsoon Rainfall (EIMR) index includes precipitation over the neighbouring oceans and land that are affected by the Indian monsoon (Goswami et al., 1999). The EIMR index is the average precipitation per day over the area 70°E - 110°E, 10°N - 30°N. As well as the precipitation-based index, the Monsoon Hadley Index (MHI) represents the strength of the Indian summer monsoon circulation by measuring the shear of meridional wind between the lower and upper troposphere averaged over the same region as the EIMR index (70°E - 110°E, 10°N - 30°N). Large positive values of MHI indicate a strong monsoon with negative values corresponding to a weak monsoon (Fig 9).

In Fig. 9b and c the points indicate the average index for the summer months for each interglacial for the last 100 years of the simulation. The bars either side show the summer minimum and maximum indices throughout the 100 simulated years. Both the EIMR and MHI indices are higher in KM5c than the pre-industrial simulation for the summer months, indicating a stronger summer monsoon in the simulation for KM5c than the pre-industrial. Looking to Fig. 3 and 4, the terrestrial areas have overall higher SATs and precipitation in the JJAS summer months. Although the Hadley circulation is predicted to be stronger in KM5c than the pre-industrial (as seen in the MHI (Fig. 9c), the simulated changes in surface winds are small between KM5c and pre-industrial, with slight decreases in wind strength across the eastern Arabian Sea and India simulated in summer months. The increased surface winds moving from Somalia into the Middle East in KM5c, compared to pre-industrial, is the only area where increased summer monsoon winds are simulated in KM5c (Fig 3c). The higher SAT simulated over terrestrial areas in summer is not seen over India where increased cloud cover counteracts the increased insolation in this area (Fig 3a). This, combined with an increase in SSTs in KM5c summer compared to pre-industrial, decreases the pressure gradient between ocean and land causing weaker winds moving from the Arabian Sea into India, despite higher precipitation still simulated over most of the Indian sub-continent in summer.

As KM5c has an orbital forcing very close to modern, any changes between the Indian monsoon in KM5c and the pre-industrial simulation are largely due to the implementation of other boundary conditions. The difference in the simulated Indian monsoon is likely due to the higher CO_2 forcing in the Pliocene simulations. It has been well established in the literature that increases in greenhouse gas concentrations intensify the Asian summer monsoon due to enhanced moisture transport into the Asian monsoon region (Kitoh et al., 1997; Annamalai et al., 2007; Kripalani et al., 2007). The higher moisture capacity of warmer air (a rate of 6-7% increase per degree) as defined by the Clausius-Clapeyron equation, is responsible for the observed intensified precipitation (Xie et al., 2014). This increase in seasonal precipitation, even in regions of weaker flow, has been noted in the literature since Kitoh et al. (1997) described weakening of the low level monsoon winds over the Arabian sea despite an increase in summer monsoon rainfall over India. Increased summer precipitation over India, with no change or weakened surface winds, has been reproduced in other modelling studies for future climate change (May, 2002; Ueda et al., 2006), and has been shown using HadCM3 with doubled CO_2 (Turner et al., 2007).

The main difference forcing a stronger Indian monsoon in the KM5c experiment compared to the pre-industrial, is higher CO_2 causing high temperatures and enhanced moisture transport and therefore higher levels of precipitation. To keep this investigation consistent with previous modelling studies such as Prescott et al. (2014) and the PlioMIP project, the CO_2 value was chosen to be 405ppm. Estimates of CO_2 for the Piacenzian have been in the range 305-415ppm (Pagani et al., 2009) with a more recent estimate suggesting a range of 280 – 420 ppm (Martínez-Botí et al., 2015). The CO_2 concentration is kept at 405ppm for all the experiments in this study. While it has been demonstrated that the CO_2 levels varied throughout the Pliocene and would have had an influence on the intensity of the Indian Monsoon. These variations have not been accounted for in this study as CO_2 records for the Pliocene capable of resolving variability over orbital timescales are still emerging.

4.2 How does the simulation of the Indian monsoon change when simulating three further Pliocene interglacials with orbital forcing substantially different to modern?

G17, K1 and KM3 are negative isotope excursions of similar magnitude, however when compared to KM5c, the magnitude of temperature, precipitation and pressure differences over the monsoon area in G17 is much smaller in JJAS than K1 and KM3. The differences between the interglacials are due to orbital forcing; K1 and KM3 display very similar summer signals, and both have stronger precession forcing than G17. In K1 and KM3, the northern hemisphere receives 10% and 6% respectively more summer insolation than the pre-industrial simulation compared to 1% in G17 and only 0.1% in KM5c. The EIMR and MHI follow the same pattern of distribution with the indices for the pre-industrial being consistently lowest, as an average as well as minimum and maximum (Table 1; Fig. 9). The pattern of average EIMR and MHI follow the same pattern as the average Northern Hemisphere insolation. The interglacials with the highest average EIMR index (K1 and KM3), and therefore strongest average monsoon, also result in the largest difference between the maximum and minimum EIMR, with the opposite being the case for the pre-industrial simulation and KM5c interglacial, which indicates a weaker monsoon signal. This suggests the stronger precession forcing causes, on average, higher rainfall and a stronger monsoon, but also a larger spread of possible monsoon strengths. The MHI similarly shows this pattern with the difference between minimum and maximum MHI in K1 and KM3 larger than G17 and KM5c. The minimum summer MHI for pre-industrial, however is lower than the other simulations at -1.8 ms^{-1} which corresponds to a weak summer monsoon (Fig. 9). However, direct comparison of maximum and minimum values between the MHI and EMIR indices is difficult given the different methodological approaches to monsoon estimation that each technique employs.

G17, K1 and KM3 are all simulated to have higher precipitation over both terrestrial areas and the surrounding ocean, with northern Indian summer precipitation levels in K1 and KM3 reaching 13 and 11mm/day more than KM5c respectively. While strong increases in summer SAT are simulated over the terrestrial areas particularly in K1 and KM3, these temperature increases are not seen over India specifically. Increases in cloud cover reduce the amount of solar radiation reaching the surface in this area and enhanced precipitation increases evaporative cooling.

The reduced temperature and pressure gradients over India cause a reduction in wind speed across the Arabian Sea and Bay of Bengal in the interglacials, as also discussed above between KM5c and pre-industrial. The increases in precipitation over the Indian ocean during summer follow a ‘warmer-gets-wetter’ pattern (Xie et al., 2010; Huang et al., 2013), whereby SST patterns are the dominant mechanism for tropical precipitation response in areas where local warming in SSTs exceeds the tropical average (Xie et al., 2014). The results presented for orbital configurations specific to the individual interglacial events studied are supported by more idealised orbital forcing experiments completed by Bosmans et al. (2018).

All the interglacials display higher summer SSTs over the Indian Ocean than pre-industrial by ~2°C in KM5c and 3°C and higher in G17, K1 and KM3. Proxy data from monsoon areas can be used to compare these average changes; Dowsett et al. (2013) compared SSTs between the PlioMIP ensemble and the PRISM3 reconstruction. The PRISM SSTs used in the comparison have undergone a warm peak average method (Dowsett & Poore, 1991) to develop an 'average interglacial' for the mPWP. ODP sites 709, 716, 722 and 758 in the Indian Monsoon area have been assigned 'high confidence' using the λ-confidence scheme (Dowsett et al., 2012), and despite representing an average warm interglacial still reconstruct lower SSTs than the multi-model mean (MMM) at all sites, suggesting that the models in the PlioMIP1 ensemble may overestimate SSTs in this area. HadCM3 specifically, simulates the highest SSTs out of the MMM at all these sites, simulating approximate 2°C higher than the PRISM SST reconstruction. The 2°C and 3°C SST warming simulated in the interglacials in this study therefore may be too high due to a warm bias in HadCM3 over this area. Overly warm SSTs would influence the simulation of the monsoon such as reducing the pressure and temperature gradient between the land and ocean and reducing wind speed. However, caution should be applied when interpreting this as due to the time slab nature of the PRISM SSTs, there is the potential that the PRISM data does not capture the interglacial peaks that have been simulated in this study.

The data-model discord in SSTs is not solely seen in the Indian monsoon area but has also been noted throughout the low latitudes. In line with current understanding, the higher CO_2 concentration in the Pliocene would be expected to cause warmer tropical SSTs, which is the temperature pattern simulated by climate models. Data reconstructions find tropical SSTs to be little or no warmer than present day (Haywood et al., 2016). However, interpretation of the proxy data in the Pliocene is evolving. Recent work by O'Brien et al. (2014) and Evans et al. (2016) detailed the impact of changing seawater chemistry on Mg/Ca derived SST estimates and found that the previous SST reconstructions to be underestimated. The alkenone proxy reaches saturation at about 28°C which inhibits its use for producing records from the warmest locations. Faunal assemblage techniques (used to determine the SST estimates in the Indian monsoon area) can be affected by increased dissolution in the warm end members of assemblages which result in cooler SST estimates. Overall, these uncertainties in SST reconstructions highlight the need for further study before concrete conclusions can be drawn about the models ability to simulate SST in this area.

Here, the simulated differences in SAT, precipitation, MSLP and salinity are larger between K1 and KM3, and KM5c, where the only difference is orbital forcing, than they are between the pre-industrial simulation and KM5c, where Pliocene boundary conditions have been implemented. This shows the high potential for orbital forcing to affect the strength of the Indian summer monsoon, especially in addition to Pliocene boundary conditions that already cause intensified Indian summer monsoon due to increased CO_2. This is in line with previous work as far back as Prell and Kutzbach (1992) in a study to identify the sensitivity of the Indian monsoon to various boundary conditions showed the monsoon is most sensitive to elevation and orbital changes. As the simulations for the mPWP interglacials in this manuscript use a topography not dissimilar to modern it would follow that the interglacials with very different orbital forcing caused a more significant change in Indian monsoon than the rest of the changed Pliocene boundary conditions combined.

4.3 What does the modelled variability in the Indian monsoon behaviour imply about interpreting discrete and often time specific proxy records of Indian monsoon behaviour?

It is not currently possible to compare the specific interglacial time slices with geological data due to insufficient dating and chronological control. In general, the trends seen in the proxy data suggest that the Pliocene simulations should show a stronger monsoon than modern, and this is reflected in the Indian monsoon EIMR and MHI indices for all simulated interglacials.

KM5c does have a stronger summer Indian monsoon than pre-industrial but this signal is surpassed by the signals in G17, K1 and KM3 due to the strong precession especially in K1 and KM3. This could be important for proxy reconstructions with a large signal of increased monsoon strength in the Pliocene but without the temporal resolution to pinpoint when in time that was. Such records could incorrectly interpret the large signal as relevant for the whole Pliocene and potentially, future climate change. In contrast, this study finds that orbital forcing has a large effect on the Pliocene Indian monsoon, and therefore any assumptions about future monsoon behaviour based on the Pliocene need to concentrate on interglacials when the pattern of orbital was the same, or very similar, to today. An obvious target for this is KM5c that has a very near modern orbit and HadCM3 simulates a stronger summer Indian monsoon than the pre-industrial. KM5c (3.205 Ma) is now the focus for modelling and data efforts within PlioMIP2.

A caveat of this study is the uncertainty surrounding the topography of the Tibetan Plateau. Model simulations by Prell and Kutzbach (1992) showed clearly that the uplift of the Tibetan Plateau had had dramatic effects on the Indian monsoon. The PRISM3D topography used as the boundary condition for the experiments presented in this study has the elevation of the Tibetan Plateau kept at approximately modern values (Sohl et al., 2009). However, there is some uncertainty about whether the Tibetan Plateau had reached near modern elevation by the Miocene or Pliocene. Most evidence seems to suggest the Tibetan Plateau reached its modern height by ~3.6 Ma, which is before the interglacials simulated in this study. A recent high resolution ostracod record from Lake Qinghai of the northeast margin of the Tibetan Plateau found that the deep lacustrine ostracod fauna disappeared abruptly at ~3.6 Ma (Lu et al., 2017), and the sediment lithology from Lake Qinghai changed from deep lacustrine sub-facies to a shallower facies also at this time (Fu et al., 2013). The authors attribute these changes to uplift of the Qinghai Nanshan, indicating an overall extension of north-eastern Tibetan Plateau at ~3.6 Ma (Lu et al., 2017). Therefore, if the uplift did occur after 3.6 Ma the elevation of the Tibetan Plateau used in the simulations may be too high and model could therefore be simulating stronger monsoons than is realistic. However, the overall effect of the uncertainty created by a partially constrained uplift history would highly depend on the specific character of the true uplift itself (Boos et al., 2010; Zhang et al., 2015).

4.4 Future work

Here, the Indian monsoon is simulated for four interglacials in the Piacenzian. To understand a more complete picture of monsoon variability throughout this time, it would be informative to also simulate the Indian monsoon in cooler or glacial events in the Piacenzian, as well as interglacial events with different orbital configurations than those used here. In particular a simulation using an extreme precession maximum would be a useful addition to the experiments performed. While this study has looked at interglacial monsoon variability on orbital timescales, there are also short-term changes in monsoon intensity on sub-orbital timescales. For example, variability due to oscillations in the thermohaline circulation, atmospheric energy and moisture transfer all happen on decadal timescales (Wang et al., 2005) and would create a more complete picture of potential Pliocene monsoon variability. More proxy reconstructions from the monsoon area with the temporal resolution necessary to be able to compare to these simulations would further this analysis. The PlioMIP2 project, which is performing simulations with the orbital forcing for KM5c, is a further opportunity for the investigation of the mid-Piacenzian monsoons with an ensemble of models and would also reduce potential for model bias.

5. Conclusions

This paper presents climatological outputs for four interglacials in the mPWP (MIS G17, K1, KM3, KM5c) for the summer Indian monsoon using HadCM3. MIS KM5c has a near modern orbit (Fig. 2) and monsoon indices indicate a slightly stronger Indian summer monsoon and increased SAT and precipitation over terrestrial areas. These changes are due to a higher CO_2 concentration of 405ppm in the simulation for KM5c. The very different-from-modern orbital forcing in the other three interglacials, especially MIS K1 and KM3, triggers a stronger climate signal and resulting change in the simulated nature of the Indian summer monsoon. The results from this paper suggest that the orbital forcing during MIS K1 and KM3 may force a more variable summer monsoon, as well as, on average, a stronger summer monsoon. This shows the significant potential for orbital forcing (especially precession), to affect the Indian summer monsoon, particularly when simulated with mPWP boundary conditions and higher CO_2. To be robust, assertions of analogous behaviour between Pliocene and future monsoons must first account for time specific orbital forced variations in monsoon behaviour during the Pliocene. If the focus of geological reconstructions from the mPWP is to understand the Indian summer monsoon in a warmer, higher CO_2 world of relevance to future climate change, our results indicate a strong influence of insolation in simulating the Indian monsoon during the mPWP. Therefore, great care should be taken when interpreting Pliocene geological records in terms of understanding future monsoon behaviour and should concentrate on interglacial events in the Pliocene when orbital forcing was the same or very similar to today, such as MIS KM5c.

Acknowledgements

All authors acknowledge receipt of funding from the European Research Council under the European Union's Seventh Framework Programme (FP7/2007-2013)/ERC grant agreement no. 278636. The authors also gratefully acknowledge comments made by the two anonymous reviewers and by Dr Samantha R Cook.

References

Annamalai, H., Hamilton, K., Sperber, K.R., Annamalai, H., Hamilton, K. & Sperber, K.R. (2007). The South Asian Summer Monsoon and Its Relationship with ENSO in the IPCC AR4 Simulations. Journal of Climate, 20, (6). 1071–1092.

Ao, H., Roberts, A.P., Dekkers, M.J., Liu, X., Rohling, E.J., Shi, Z., An, Z. & Zhao, X. (2016). Late Miocene–Pliocene Asian monsoon intensification linked to Antarctic ice-sheet growth. Earth and Planetary Science Letters, 444, 75-87.

Berger, A. (1988). Milankovitch Theory and climate. Reviews of Geophysics, 26, (4). p.p. 624.

Berger, A.L. (1978). Long-Term Variations of Caloric Insolation Resulting from the Earth’s Orbital Elements. Quaternary Research, 9, (2), 139–167.

Boos, W. R., and Kuang, Z. M. (2010). Dominant control of the South Asian monsoon by orographic insulation versus plateau heating. Nature, 463, 218–222.

Bosmans, J.H.C., Erb, M. P., Dolan, A.M., Drijfhout, S.S., Tuenter, E., Hilgen, F.J., Edge, D., Pope,

J. O. & Lourens, L.J. (2018). Response of the Asian summer monsoons to idealized precession and obliquity forcing in a set of GCMs. Quaternary Science Reviews, 188, 121-135.

Braconnot, P., Joussaume, S., Marti, O. & de Noblet, N. (1999). Synergistic feedbacks from ocean and vegetation on the African Monsoon response to Mid-Holocene insolation. Geophysical Research Letters, 26, (16), 2481–2484.

Braconnot, P. & Marti, O. (2003). Impact of precession on monsoon characteristics from coupled ocean atmosphere experiments: changes in Indian monsoon and Indian ocean climatology. Marine Geology, 201, (1). 23–34.

Braconnot, P., Marzin, C., Grégoire, L., Mosquet, E. & Marti, O. (2008). Monsoon response to changes in Earth's orbital parameters: comparisons between simulations of the Eemian and of the Holocene. Clim. Past, 4, 281–294.

Bragg, F.J., Lunt, D.J. & Haywood, A.M. (2012). Mid-Pliocene climate modelled using the UK Hadley Centre Model: PlioMIP Experiments 1 and 2. Geoscientific Model Development Discussions, 5, (2), 837–871.

Chang, Z., Xiao, J., Lü, L. & Yao, H. (2010). Abrupt shifts in the Indian monsoon during the Pliocene marked by high-resolution terrestrial records from the Yuanmou Basin in southwest China. Journal of Asian Earth Sciences, 37, (2). 166–175.

Chen, J., Chen, Y., Liu, L., Ji, J., Balsam, W., Sun, Y. & Lu, H. (2006). Zr/Rb ratio in the Chinese loess sequences and its implication for changes in the East Asian winter monsoon strength. Geochimica et Cosmochimica Acta, 70, (6). 1471–1482.

Christensen, J.H., Kumar, K.K., Aldrian, E., An, S.-I., Cavalcanti, I.F.A., De Castro, M., Dong, W., Goswami, P., Hall, A., Kanyanga, J.K., Kitoh, A., Kossin, J., Lau, N.-C., Renwick, J., Stephenson, D.B., Xie, S.-P. & Zhou, T. (2013). Climate Phenomena and their Relevance for Future Regional Climate Change. In: T. F. Stocker, D. Qin, G.-K. Plattner, M. Tignor, S. K. Allen, J. Boschung, A. Nauels, Y. Xia, V. Bex, & P. M. Midgley (eds.). Climate Change 2013 - The Physical Science Basis. Contribution of Working Group 1 to the Fifth Assessment Report of the International Panel on Climate Change. Cambridge, United Kingdom and New York, NY, USA: Cambridge University Press, 1217–1308.

Clemens, S.C. & Prell, W.L. (1990). Late Pleistocene variability of Arabian Sea summer monsoon winds and continental aridity: Eolian records from the lithogenic component of deep-sea sediments. Paleoceanography, 5, (2), 109–145.

Clift, P.D. & Plumb, R.A. (2008). The Asian Monsoon, Causes History and Effects. Cambridge University Press.

Cox, P.M., Betts, R.A., Bunton, C.B., Essery, R.L.H., Rowntree, P.R. & Smith, J. (1999). The impact of new land surface physics on the GCM simulation of climate and climate sensitivity. Climate

Dynamics, 15, (3), 183–203.

Cox, P.M. (2001). Description of the "TRIFFID" Dynamic Global Vegetation Model. Hadley Centre Technical Note, 24, 1-17.

deMenocal, P.B. & Rind, D. (1993). Sensitivity of Asian and African climate to variations in seasonal insolation, glacial ice cover, sea surface temperature, and Asian orography. Journal of Geophysical Research, 98 (D4), 7265.

Ding, Z.L., Yang, S.L., Sun, J.M. & Liu, T.S. (2001). Iron geochemistry of loess and red clay deposits in the Chinese Loess Plateau and implications for long-term Asian monsoon evolution in the last 7.0 Ma. Earth and Planetary Science Letters, 185, (1), 99–109.

Dowsett, H., Robinson, M., Haywood, A.M., Salzmann, U., Hill, D., Sohl, L., Chandler, M., Williams, M., Foley, K. & Stoll, D. (2010). The PRISM3D paleoenvironmental reconstruction. Stratigraphy. 7, (2-3), 123-139.

Dowsett, H.J., Foley, K.M., Stoll, D.K., Chandler, M.A., Sohl, L.E., Bentsen, M., Otto-Bliesner, B.L., Bragg, F.J., Chan, W.-L., Contoux, C., Dolan, A.M., Haywood, A.M., Jonas, J.A., Jost, A., Kamae, Y., Lohmann, G., Lunt, D.J., Nisancioglu, K.H., Abe-Ouchi, A., Ramstein, G., Riesselman, C.R., Robinson, M.M., Rosenbloom, N.A., Salzmann, U., Stepanek, C., Strother, S.L., Ueda, H., Yan, Q. & Zhang, Z. (2013). Sea surface temperature of the mid-Piacenzian ocean: a data-model comparison. Scientific reports, 3.

Dowsett, H.J. & Poore, R.Z. (1991). Pliocene sea surface temperatures of the north atlantic ocean at 3.0 Ma. Quaternary Science Reviews, 10, (2–3), 189–204.

Dowsett, H.J., Robinson, M.M., Haywood, A.M., Hill, D.J., Dolan, A.M., Stoll, D.K., Chan, W.-L., Abe-Ouchi, A., Chandler, M.A., Rosenbloom, N.A., Otto-Bliesner, B.L., Bragg, F.J., Lunt, D.J., Foley, K.M. & Riesselman, C.R. (2012). Assessing confidence in Pliocene sea surface temperatures to evaluate predictive models. Nature Climate Change, 2 (5), 365–371.

Evans, D., Brierley, C., Raymo, M.E. & Wuller, W. (2016). Planktic foraminifera shell chemistry response to seawater chemistry: Pliocene-Pleistocene seawater Mg/Ca, temperature and sea level change. Earth and Planetary Science Letters, 438, 139-148.

Fu, C., An, Z., Qiang, X., Bloemendal, J., Song, Y. & Chang, H. (2013). Magnetostratigraphic determination of the age of ancient Lake Qinghai, and record of the East Asian monsoon since 4.63 Ma. Geology, 41, (8), 875–878.

Gadgil, S., Vinayachandran, P. & Francis, P. (2003). Droughts of the Indian summer monsoon: Role of clouds over the Indian Ocean. Current Science, 85, (12), 1713-1719.

Gordon, C., Cooper, C., Senior, C.A., Banks, H., Gregory, J.M., Johns, T.C., Mitchell, J.F.B. & Wood, R.A. (2000). The simulation of SST, sea ice extents and ocean heat transports in a version of the Hadley Centre coupled model without flux adjustments. Climate Dynamics, 16, (2–3),

147–168.
Goswami, B.N., Krishnamurthy, V. & Annmalai, H. (1999). A broad-scale circulation index for the interannual variability of the Indian summer monsoon. Quarterly Journal of the Royal Meteorological Society, 125, (554), 611–633.
Gupta, A.K. & Anderson, D.M. (2005). Mysteries of the Indian Ocean Monsoon System. Geological Society of India, 65, (1). 54–60.
Gupta, A.K. & Thomas, E. (2003). Initiation of Northern Hemisphere glaciation and strengthening of the northeast Indian monsoon: Ocean drilling program site 758, eastern equatorial Indian Ocean, Geology, 31, (1), 47–50.
Hays, J.D., Imbrie, J. & Shackleton, N.J. (1976). Variations in the Earth's Orbit: Pacemaker of the Ice Ages. Science, 194, (4270), 1121–1132.
Haywood, A.M., Dowsett, H.J. & Dolan, A.M. (2016). Integrating geological archives and climate models for the mid-Pliocene warm period. Nature Communications. 7.
Haywood, A.M., Dowsett, H.J., Otto-Bliesner, B., Chandler, M.A., Dolan, A.M., Hill, D.J., Lunt, D.J., Robinson, M.M., Rosenbloom, N., Salzmann, U. & Sohl, L.E. (2010). Pliocene Model Intercomparison Project (PlioMIP): experimental design and boundary conditions (Experiment 1). Geoscientific Model Development, 3, (1), 227–242.
Haywood, A.M., Hill, D.J., Dolan, A.M., Otto-Bliesner, B.L., Bragg, F., Chan, W.-L., Chandler, M.A., Contoux, C., Dowsett, H.J., Jost, A., Kamae, Y., Lohmann, G., Lunt, D.J., Abe-Ouchi, A., Pickering, S.J., Ramstein, G., Rosenbloom, N.A., Salzmann, U., Sohl, L., Stepanek, C., Ueda, H., Yan, Q. & Zhang, Z. (2013). Large-scale features of Pliocene climate: results from the Pliocene Model Intercomparison Project. Climate of the Past, 9, (1), 191–209.
Haywood, A.M. & Valdes, P.J. (2004). Modelling Pliocene warmth: contribution of atmosphere, oceans and cryosphere. Earth and Planetary Science Letters, 218, (3–4), 363–377.
Huang, P., Xie, S.-P., Hu, K., Huang, G. & Huang, R. (2013). Patterns of the seasonal response of tropical rainfall to global warming. Nature Geoscience, 6, (5), 357–361.
Huang, Y., Clemens, S.C., Liu, W., Wang, Y. & Prell, W.L. (2007). Large-scale hydrological change drove the late Miocene C4 plant expansion in the Himalayan foreland and Arabian Peninsula. Geology, 35, (6), 531-534,
Kitoh, A., Yukimoto, S., Noda, A. & Motoi, T. (1997). Simulated Changes in the Asian Summer Monsoon at Times of Increased Atmospheric CO_2. Journal of the Meteorological Society of Japan. Ser. II, 75, (6), 1019–1031.
Kripalani, R.H., Oh, J.H., Kulkarni, A., Sabade, S.S. & Chaudhari, H.S. (2007). South Asian summer monsoon precipitation variability: Coupled climate model simulations and projections under IPCC AR4. Theoretical and Applied Climatology, 90, (3–4), 133–159.

Laskar, J., Robutel, P., Joutel, F., Gastineau, M., Correia, A.C.M. & Levrard, B. (2004). A long-term numerical solution for the insolation quantities of the Earth. A&A, 428, 261–285.

Li, Y., Harrison, S.P., Zhao, P. & Ju, J. (2009). Simulations of the impacts of dynamic vegetation on interannual and interdecadal variability of Asian summer monsoon with modern and mid-Holocene orbital forcings. Global and Planetary Change, 66, (3–4), 235–252.

Liddy, H.M., Feakins, S.J. & Tierney, J.E. (2016). Cooling and drying in northeast Africa across the Pliocene. Earth and Planetary Science Letters, 449, 430–438.

Lisiecki, L.E. & Raymo, M.E. (2005). A Pliocene-Pleistocene stack of 57 globally distributed benthic δ 18 O records. Paleoceanography, 20, (1), 1003

Liu, X. & Shi, Z. (2009). Effect of precession on the Asian summer monsoon evolution: A systematic review. Chinese Science Bulletin, 54, (20), 3720–3730.

Lu, F., An, Z., Chang, H., Dodson, J., Qiang, X., Yan, H., Dong, J., Song, Y., Fu, C. & Li, X. (2017). Climate change and tectonic activity during the early Pliocene Warm Period from the ostracod record at Lake Qinghai, northeastern Tibetan Plateau. Journal of Asian Earth Sciences, 138, 466–476.

Martínez-Botí, M.A., Foster, G.L., Chalk, T.B., Rohling, E.J., Sexton, P.F., Lunt, D.J., Pancost, R.D., Badger, M.P.S. & Schmidt, D.N. (2015). Plio-Pleistocene climate sensitivity evaluated using high-resolution CO_2 records. Nature, 518, (7537), 49–54.

Marzocchi, A., Lunt, D.J., Flecker, R., Bradshaw, C.D., Farnsworth, A. & Hilgen, F.J. (2015). Orbital control on late Miocene climate and the North African monsoon: insight from an ensemble of sub-precessional simulations. Clim. Past, 11, 1271–1295.

May, W. (2002). Simulated changes of the Indian summer monsoon under enhanced greenhouse gas conditions in a global time-slice experiment. Geophysical Research Letters, 29, (7). 22–24.

Mohan, K. & Gupta, A.K. (2011). Intense deep convective mixing in the Southeast Arabian Sea linked to strengthening of the Northeast Indian monsoon during the middle Pliocene (3.4 Ma). Current Science, 101, (4), 1-5.

O'Brien, C.L., Foster, G.L., Martínez-Botí, M.A., Abell, R., Rae, J.W.B. & Pancost, R.D. (2014). High sea surface temperatures in tropical warm pools during the Pliocene. Nature Geoscience, 7, (8), 606.

Overpeck, J., Anderson, D., Trumbore, S. & Prell, W. (1996). The southwest Indian Monsoon over the last 18 000 years. Climate Dynamics, 12, (3), 213–225.

Pagani, M., Liu, Z., LaRiviere, J. & Ravelo, A.C. (2009). High Earth-system climate sensitivity determined from Pliocene carbon dioxide concentrations. Nature Geoscience, 3, (1), 27–30.

Pollard, D. & Reusch, D.B. (2002). A calendar conversion method for monthly mean paleoclimate model output with orbital forcing. Journal of Geophysical Research Atmospheres, 107, (22), 4615.

Prell, W.L. & Campo, E. Van (1986). Coherent response of Arabian Sea upwelling and pollen transport to late Quaternary monsoonal winds. Nature, 323, (6088), 526–528.

Prell, W.L. & Kutzbach, J.E. (1987). Monsoon variability over the past 150,000 years. Journal of Geophysical Research, 92 (D7), 8411-8425.

Prell, W.L. & Kutzbach, J.E. (1992). Sensitivity of the Indian monsoon to forcing parameters and implications for its evolution. Nature, 360, (6405), 647–652.

Prescott, C.L., Haywood, A.M., Dolan, A.M., Hunter, S.J., Pope, J.O. & Pickering, S.J. (2014). Assessing orbitally-forced interglacial climate variability during the mid-Pliocene Warm Period. Earth and Planetary Science Letters, 400, 261–271.

Prescott, C.L., Dolan, A.M., Haywood, A.M., Hunter, S.J. & Tindall, J.C. (2018). Regional climate and vegetation response to orbital forcing within the mid-Pliocene Warm Period: A study using HadCM3. Global and Planetary Change, 161, 231-243.

Sanyal, P., Bhattacharya, S.., Kumar, R., Ghosh, S.. & Sangode, S.. (2004). Mio–Pliocene monsoonal record from Himalayan foreland basin (Indian Siwalik) and its relation to vegetational change. Palaeogeography, Palaeoclimatology, Palaeoecology, 205, (1). 23–41.

Sohl, L.E., Chandler, M.A., Schmunk, R.B., Mankoff, K., Jonas, J.A., Foley, K.M. & Dowsett, H.J. (2009). PRISM3/GISS Topographic Reconstruction. US Geological Survey Data Series, 419.

Su, T., Jacques, F.M.B., Spicer, R.A., Liu, Y.-S., Huang, Y.-J., Xing, Y.-W. & Zhou, Z.-K. (2013). Post-Pliocene establishment of the present monsoonal climate in SW China: evidence from the late Pliocene Longmen megaflora. Climate of the Past, 9 ,(4), 1911–1920.

Turner, A.G. & Annamalai, H. (2012). Climate change and the South Asian summer monsoon. Nature Climate Change, 2, (8), 587–595.

Turner, A.G., Inness, P.M. & Slingo, J.M. (2007). The effect of doubled CO_2 and model basic state biases on the monsoon-ENSO system. I: Mean response and interannual variability. Quarterly Journal of the Royal Meteorological Society, 133, (626), 1143–1157.

Ueda, H., Iwai, A., Kuwako, K. & Hori, M.E. (2006). Impact of anthropogenic forcing on the Asian summer monsoon as simulated by eight GCMs. Geophysical Research Letters, 33, (6), L06703.

Valdes, P.J., Armstrong, E., Badger, M.P.S., Bradshaw, C.D., Bragg, F., Davies-Barnard, T., Day, J.J., Farnsworth, A., Hopcroft, P.O., Kennedy, A.T., Lord, N.S., Lunt, D.J., Marzocchi, A., Parry, L.M., Roberts, W.H.G., Stone, E.J., Tourte, G.J.L. & Williams, J.H.T. (2017). The BRIDGE HadCM3 family of climate models: HadCM3@Bristol v1.0. Geoscientific Model Development, 10, 3715-3743.

Wang, B. (2006) The Asian monsoon. Springer Praxis Books, Springer, Berlin, Heidelberg.

Wang, P., Clemens, S., Beaufort, L., Braconnot, P., Ganssen, G., Jian, Z., Kershaw, P. & Sarnthein,

M. (2005). Evolution and variability of the Asian monsoon system: state of the art and outstanding issues. Quaternary Science Reviews, 24, (5), 595–629.

Wang, Y.-X., Yang, J.-D., Chen, J., Zhang, K.-J. & Rao, W.-B. (2007). The Sr and Nd isotopic variations of the Chinese Loess Plateau during the past 7 Ma: Implications for the East Asian winter monsoon and source areas of loess. Palaeogeography, Palaeoclimatology, Palaeoecology, 249, (3), 351–361.

Webster, P.J., Magaña, V.O., Palmer, T.N., Shukla, J., Tomas, R.A., Yanai, M. & Yasunari, T. (1998). Monsoons: Processes, predictability, and the prospects for prediction. Journal of Geophysical Research: Oceans, 103, (C7), 14451–14510.

Xie, S.-P., Deser, C., Vecchi, G.A., Ma, J., Teng, H., Wittenberg, A.T., Xie, S.-P., Deser, C., Vecchi, G.A., Ma, J., Teng, H. & Wittenberg, A.T. (2010). Global Warming Pattern Formation: Sea Surface Temperature and Rainfall. Journal of Climate, 23, (4), 966–986.

Xie, S., Deser, C., Vecchi, G.A., Collins, M., Tom, L., Hall, A., Hawkins, E., Johnson, N.C. & Cassou, C. (2014). Towards predictive understanding of regional climate change: Issues and opportunities for progress. Nature Climate Change. 5, 921-930.

Yan, Q., Zhang, Z.-S. & Gao, Y.-Q. (2012). An East Asian Monsoon in the Mid-Pliocene: Atmospheric and Oceanic Science Letters, 5, (6), 449-454.

Zhang, R., Yan, Q., Zhang, Z.S., Jiang, D., Otto-Bliesner, B.L., Haywood, A.M., Hill, D.J., Dolan, A.M., Stepanek, C., Lohmann, G., Contoux, C., Bragg, F., Chan, C.L., Chandler, M.A., Jost, A., Kamae, Y., Abe-Ouchi, A., Ramstein, G., Rosenbloom, N.A., Sohl, L. & Ueda, H. (2013). Mid-Pliocene East Asian monsoon climate simulated in the PlioMIP. Climate of the Past, 9, (5). 2085–2099.

Zhang, R. & Zhang, Q. (2017). Non-uniform spatial difference in the South Asian summer monsoon during the mid-Piacenzian. Atmospheric and Oceanic Science Letters, 10, (4), 269–275.

Zhang, R., Jiang, D., Zhang, Z., and Yu, E. T. (2015). The impact of regional uplift of the Tibetan Plateau on the Asian monsoon climate. Palaeogeography Palaeoclimatology Palaeoecology, 417, 137–150.

Figures and Tables:

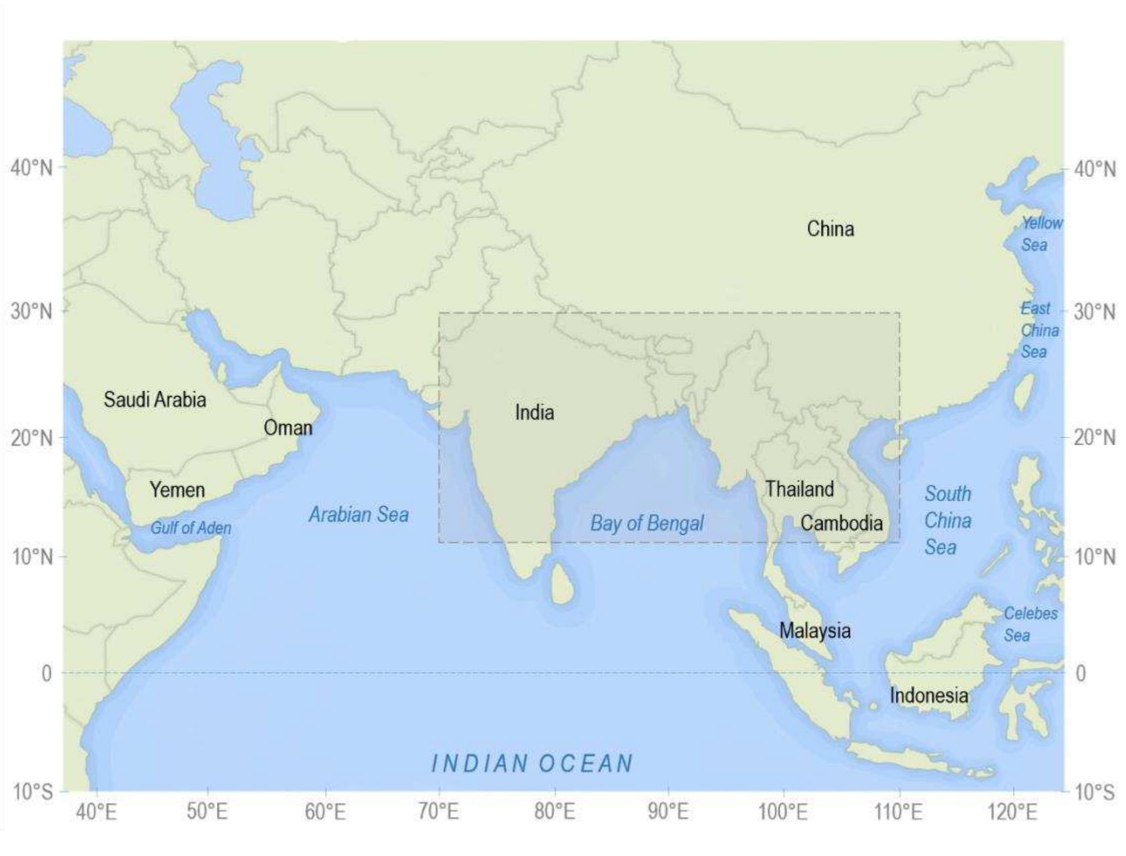

Figure 1. Map of the Indian Monsoon area. The shaded area indicating the geographical area used to calculate the monsoon indices (described in section 2.3).

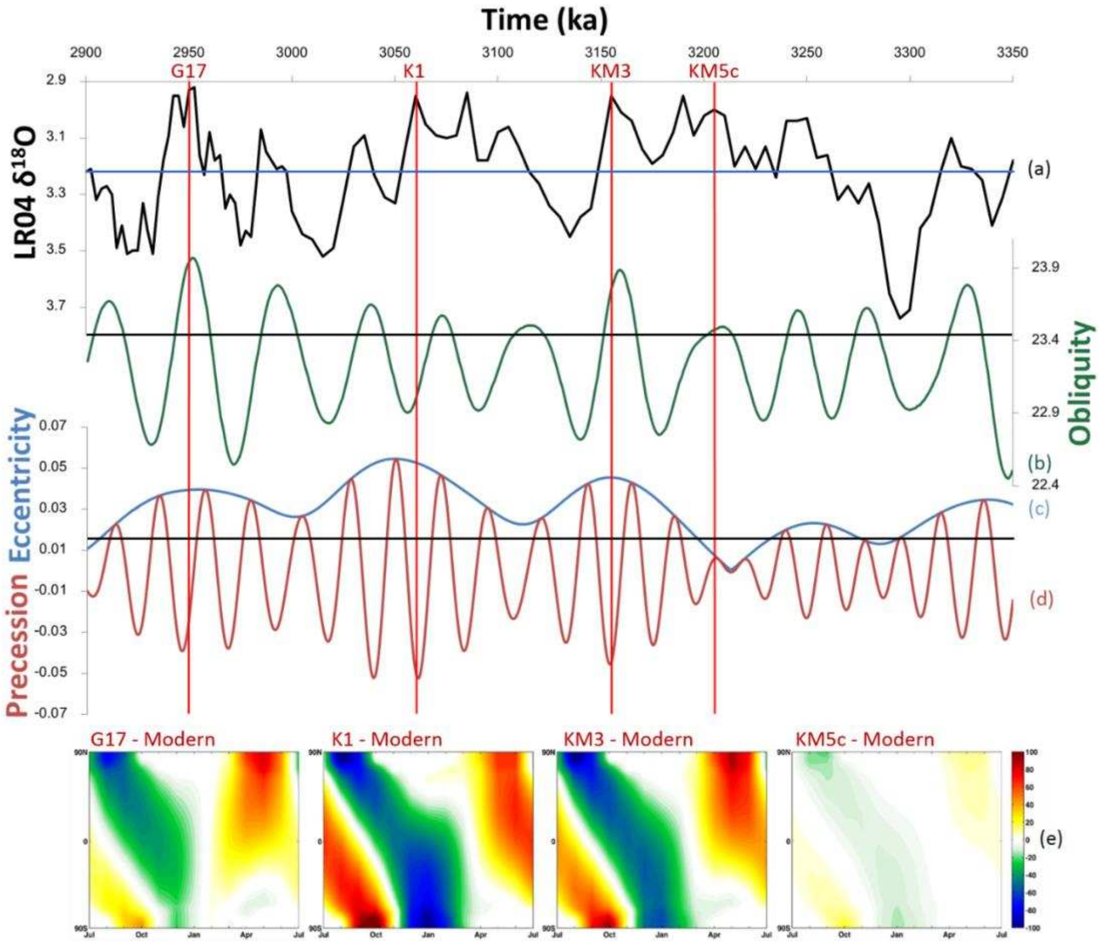

Figure 2. Marine Isotope stages (MIS) G17, K1, KM3 and KM5c plotted on (a) the benthic isotope record of Lisiecki and Raymo (2005). (b) Obliquity, (c) eccentricity, (d) precession as derived from the astronomical solution of Laskar et al. (2004). Black horizontal lines show modern orbit with blue horizontal line showing the Holocene oxygen isotope average. (e) Incoming short wave radiation flux derived from HadCM3 (Wm^{-2}) for MIS G17 minus modern; MIS K1 minus modern, MIS KM3 minus modern; MIS KM5c minus modern.

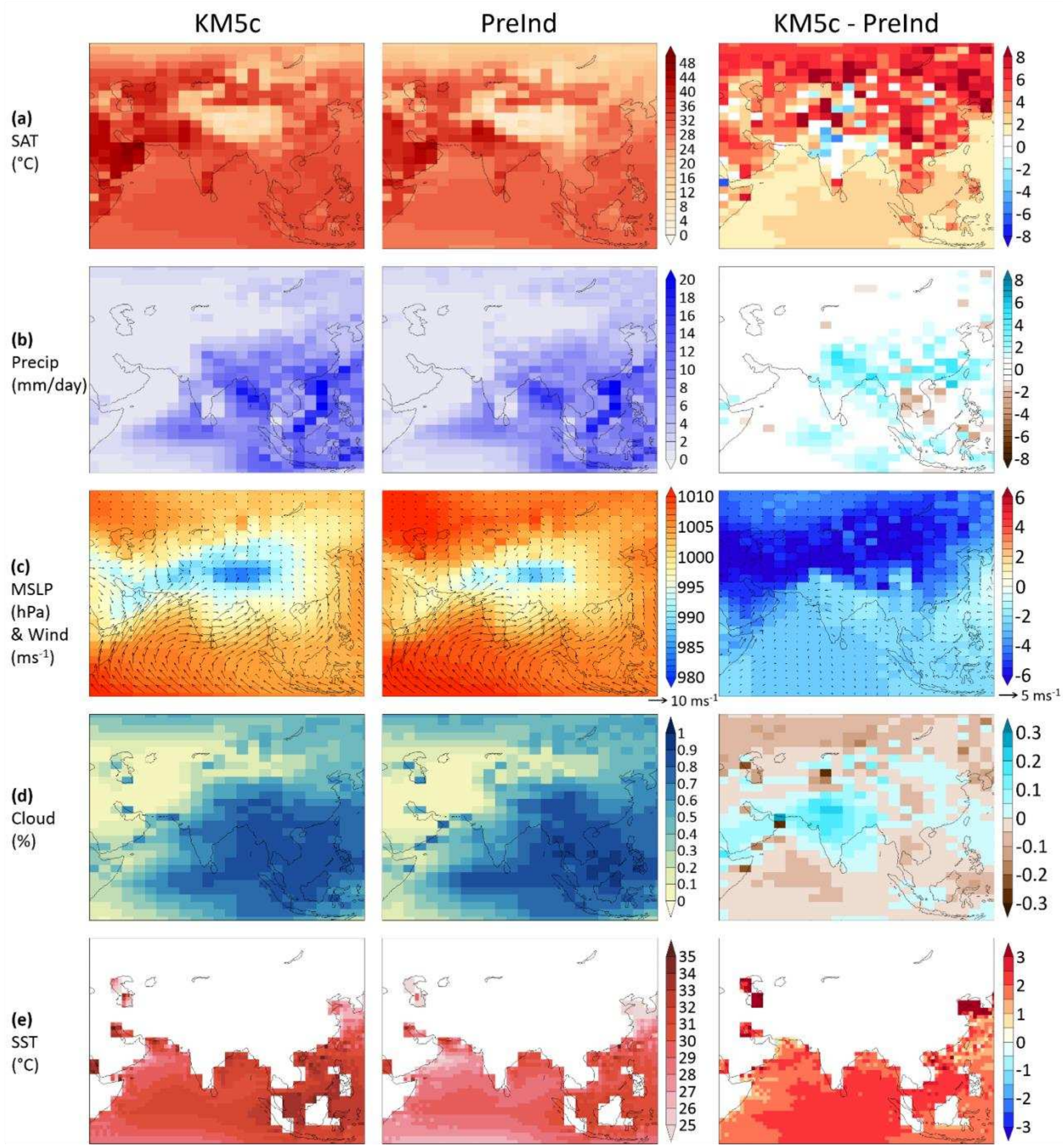

Figure 3. Left column: Average absolute JJAS (June – September) results for the MIS KM5c simulation. Middle column: Average absolute JJAS results for pre-industrial simulation. Right column: Average anomaly JJAS results for MIS KM5c minus pre-industrial, showing (a) surface air temperature (SAT) (°C), (b) precipitation (mm/day), (c) mean sea level pressure (MSLP) (hPa) and arrows showing surface winds (ms^{-1}), (d) cloud cover (%) and (e) sea surface temperatures (SSTs: °C).

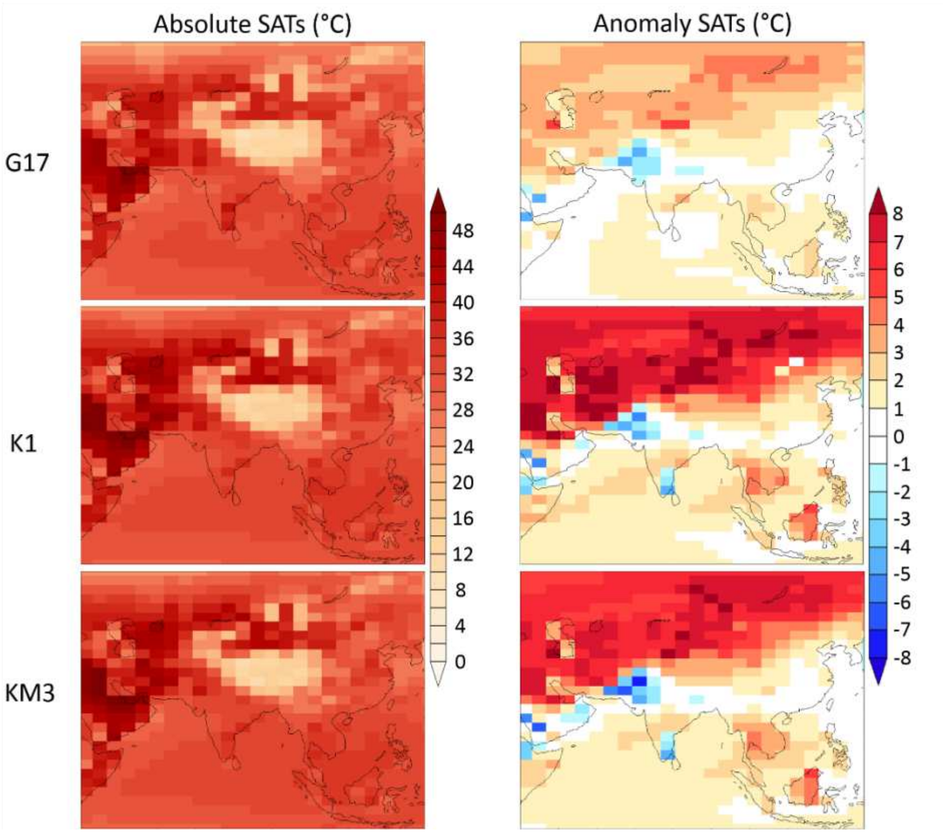

Figure 4. HadCM3 surface air temperature for JJAS (June – September) (°C). Left column: three Piacenzian interglacials (MIS G17, K1, KM3) absolute results. Right column: MIS G17, K1 and KM3 minus the MIS KM5c control.

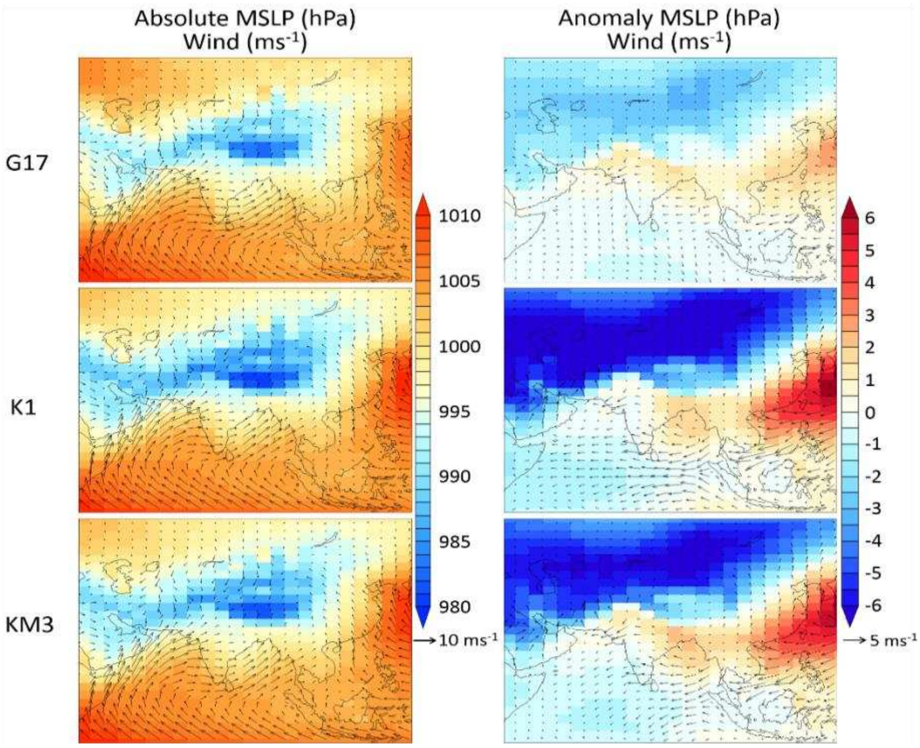

Figure 5. HadCM3 mean sea level pressure (MSLP) (hPa) for JJAS (June – September) and arrows indicating surface wind direction and strength (ms^{-1}). Left column: three Piacenzian interglacials (MIS G17, K1, KM3) absolute results. Right column: MIS G17, K1 and KM3 minus the MIS KM5c control.

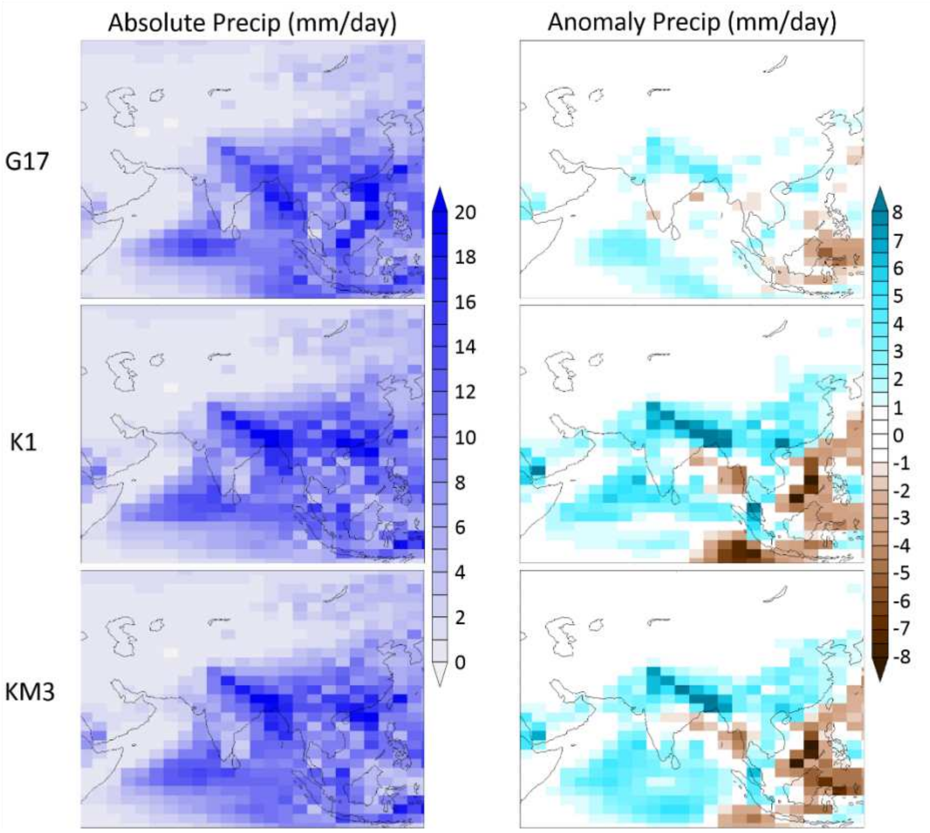

Figure 6. HadCM3 precipitation for JJAS (June – September) (mm/day). Left column: three Piacenzian interglacials (MIS G17, K1, KM3) absolute results. Right column: MIS G17, K1 and KM3 minus the MIS KM5c control.

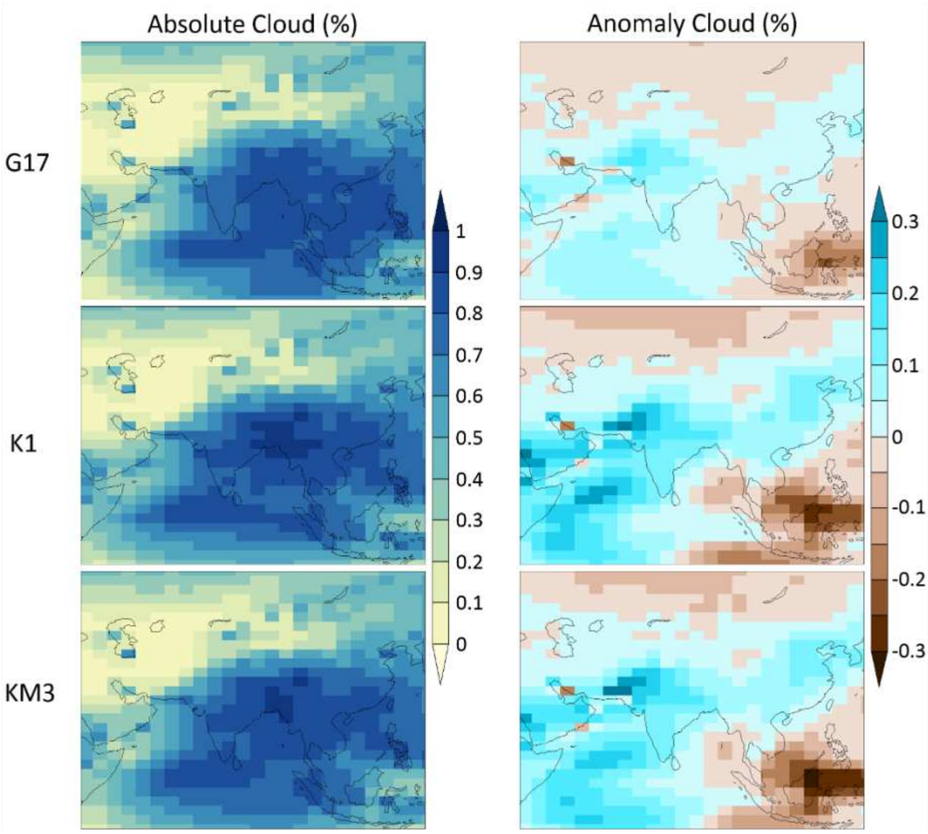

Figure 7. HadCM3 cloud cover for JJAS (June – September) (%). Left column: three Piacenzian interglacials (MIS G17, K1, KM3) absolute results. Right column: MIS G17, K1 and KM3 minus the MIS KM5c control.

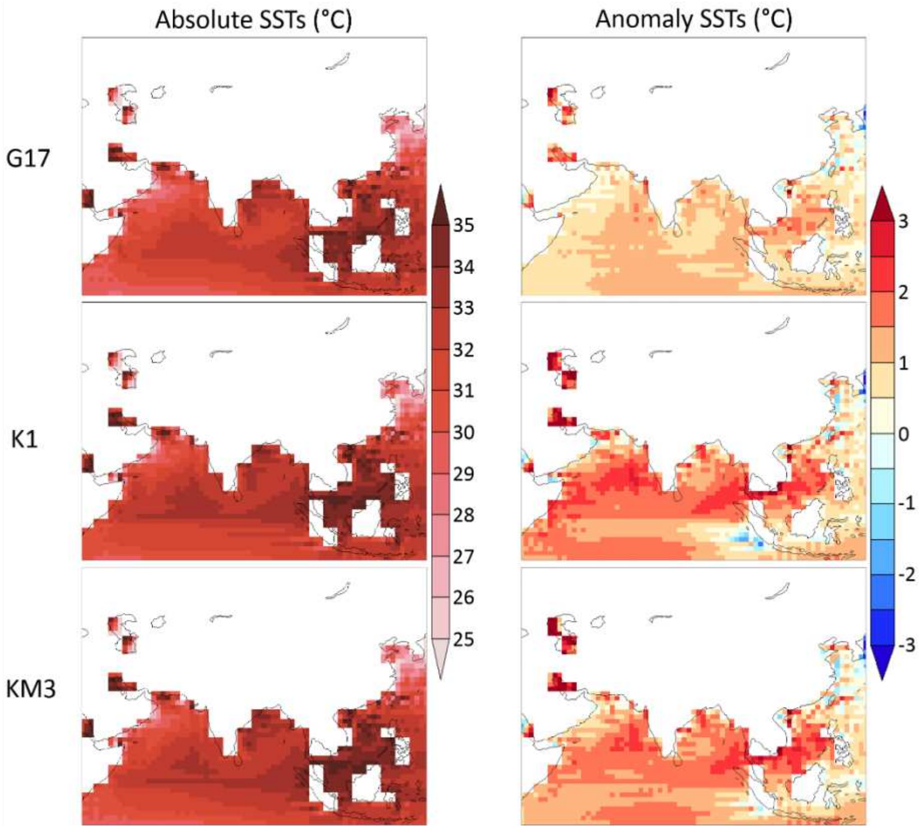

Figure 8. HadCM3 sea surface temperatures (SSTs) for JJAS (June – September) (°C). Left column: three Piacenzian interglacials (MIS G17, K1, KM3) absolute results. Right column: MIS G17, K1 and KM3 minus the MIS KM5c control.

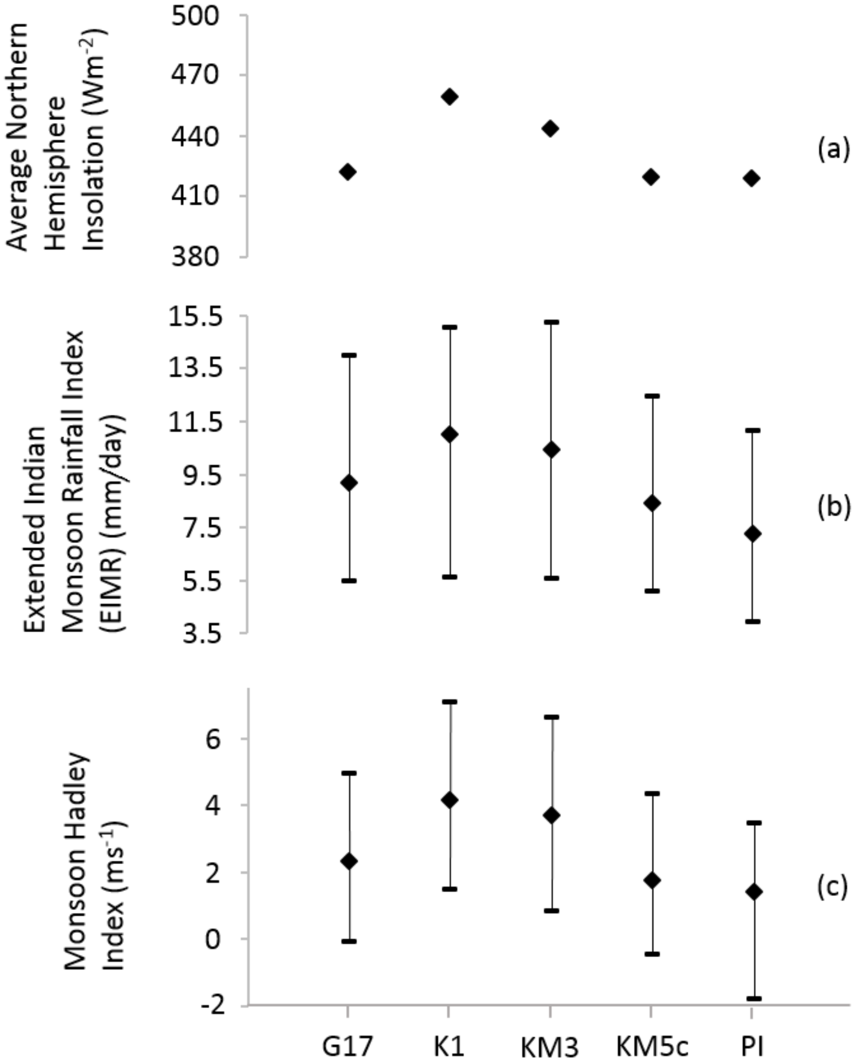

Figure 9. HadCM3 results for the four Piacenzian interglacials MIS G17, K1, KM3, KM5c and a pre-industrial simulation (PI) showing (a) the average northern hemisphere insolation (Wm^{-2}) for JJAS, (b) The Extended Indian Monsoon Rainfall (EIMR) Index (mm/day) and (c) The Monsoon Hadley Index (MHI) (ms^{-1}). In (b) and (c) diamonds indicate the 100 year average monsoon index during JJAS (June, July, August September). Bars show the minimum and maximum index throughout the 100 years for the EIMR and Monsoon Hadley Index for JJAS.

Experiment	Orbit (kyr)	CO_2 (ppmv)	Eccentricity	Precession	Obliquity	JJAS NH Insolation (Wm^{-2})	EIMR Index (mm/day)	MHI (m/s)
G17	2950	405	0.04	-0.01776	23.96	422.00	9.20	2.34
K1	3060	405	0.05	-0.05086	23.01	459.50	11.01	4.15
KM3	3155	405	0.05	-0.04350	23.76	443.40	10.44	3.69
KM5c	3205	405	0.01	0.00605	23.47	419.50	8.42	1.78
Pre-Ind	Modern	280	0.02	0.01670	23.44	419.10	7.28	1.44

Table 1. Summary of experiments including orbital parameters implemented in HadCM3 (Laskar et al., 2004), also showing average summer (June, July, August, September; JJAS) Northern Hemisphere insolation, Extended Indian Monsoon Rainfall (EIMR) index and Monsoon Hadley Index (MHI).

Supplementary Figures

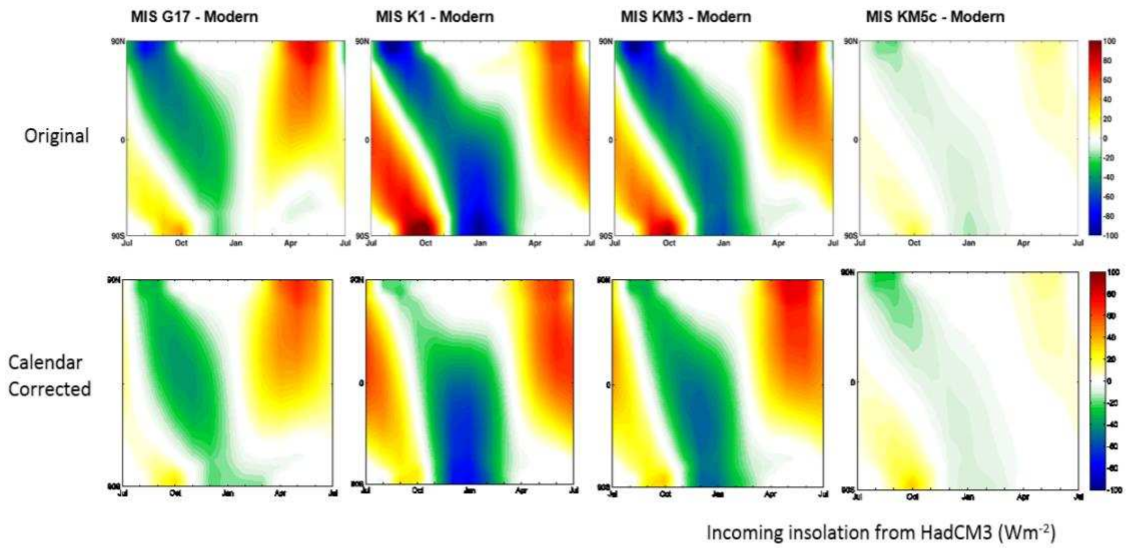

Figure S1. Incoming insolation from HadCM3 for each interglacial (MIS G17, K1, KM3 and KM5c) minus a pre-industrial simulation (modern orbit), each plot showing changing incoming insolation by month and latitude. Top row showing the original results with no calendar correction applied and bottom row showing calendar corrected incoming insolation.

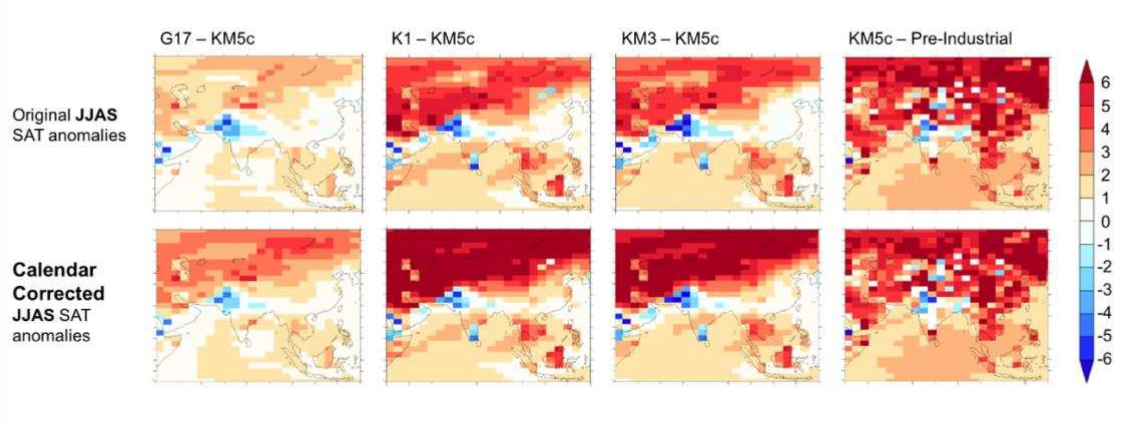

Figure S2. HadCM3 SAT anomaly (°C) for JJAS for three Piacenzian interglacials (MIS G17, K1 and KM3) minus the MIS KM5c. Far right column shows MIS KM5c minus a pre-industrial simulation. Top row indicates the original SAT results with no calendar correction applied and the bottom row the calendar corrected SAT anomalies.

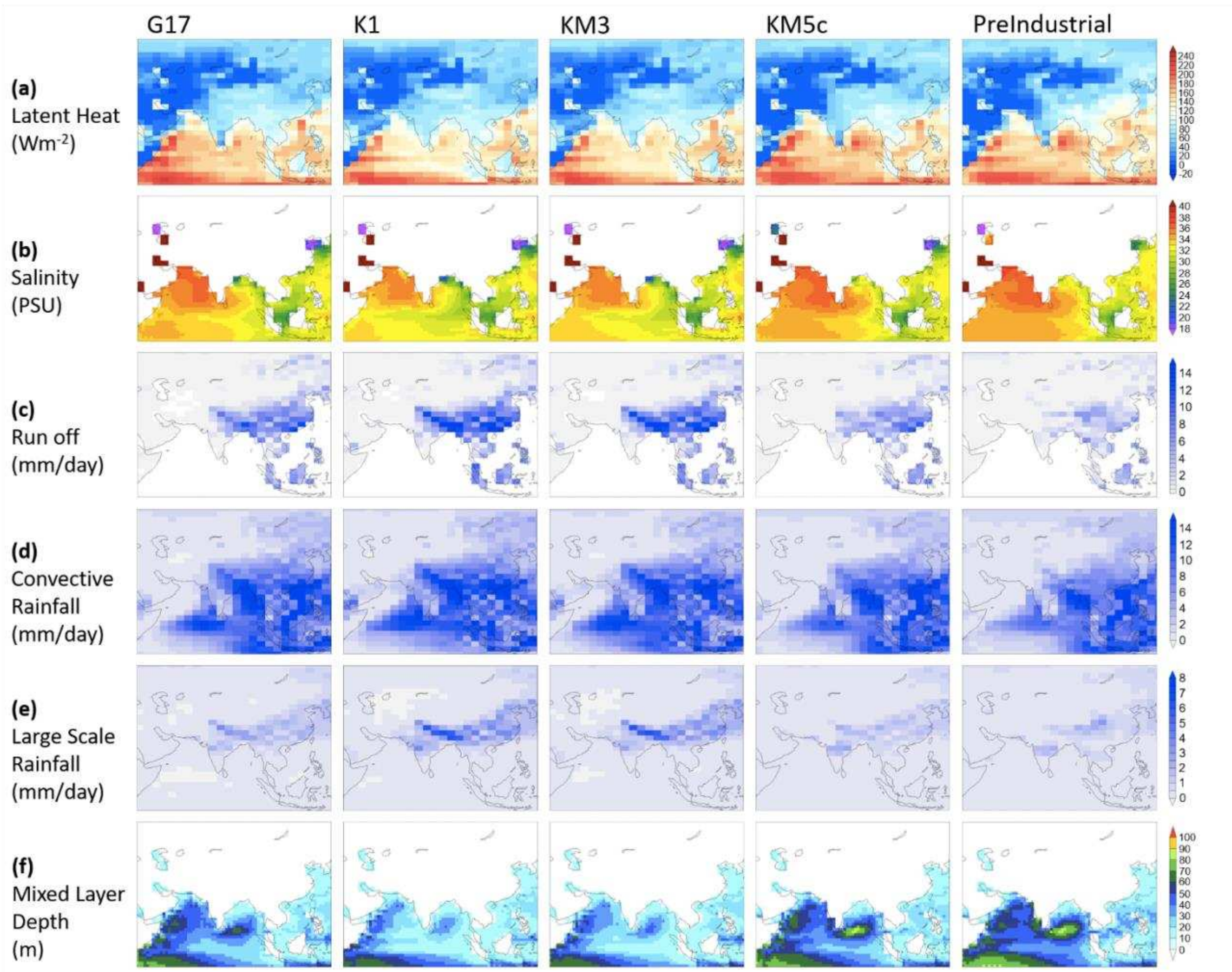

Figure S3. HadCM3 absolute results for JJAS (June, July, August, September) for four Piacenzian interglacials (MIS G17, K1, KM3 and KM5c) and a pre-industrial simulation, showing (a) Latent heat (Wm^{-2}), (b) Salinity (PSU), (c) run off (mm day^{-1}), (d) convective rainfall (mm day-1), (e) large scale rainfall (mm day^{-1}) and (f) mixed layer depth (m).

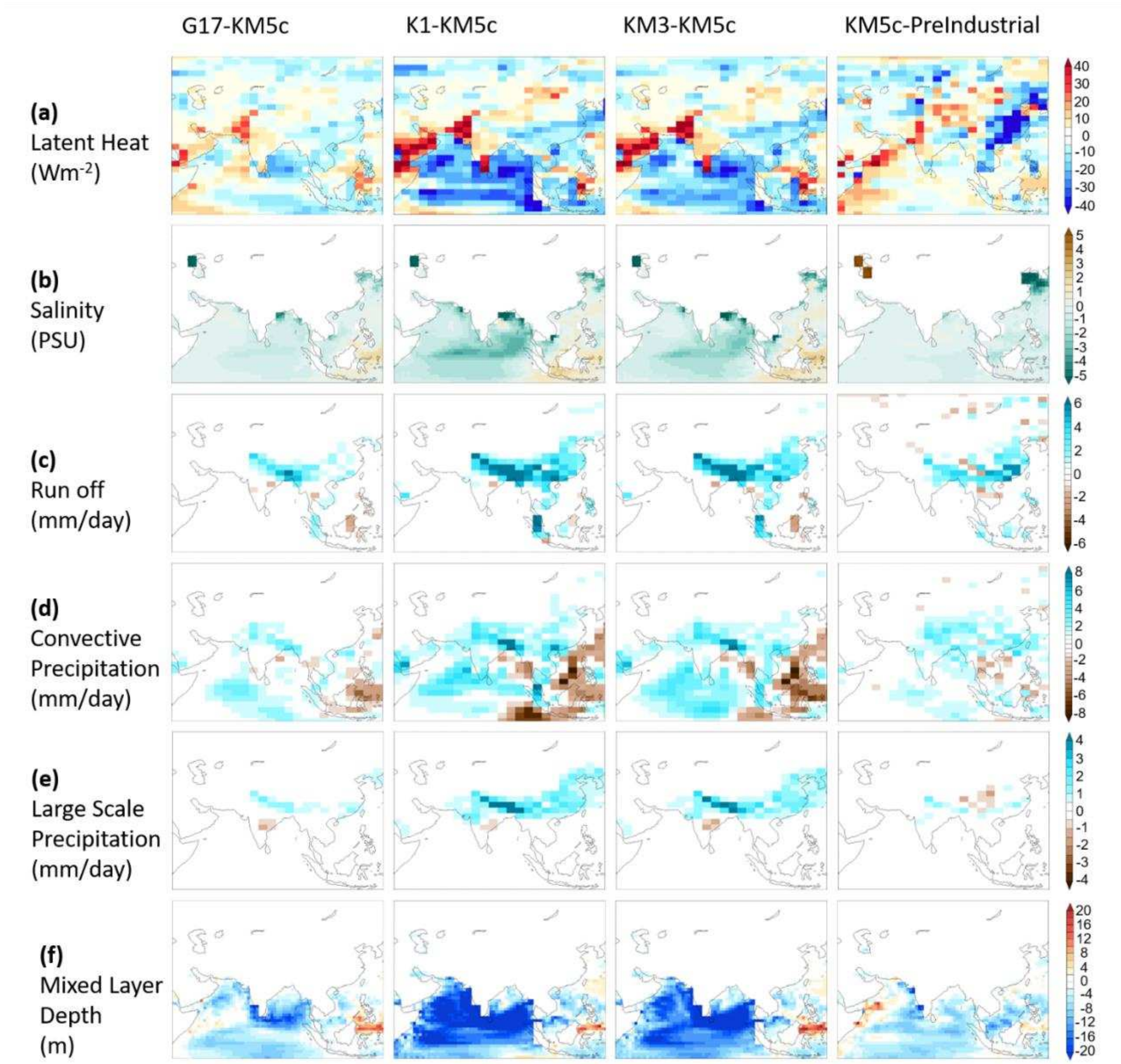

Figure S4. HadCM3 anomaly results for JJAS (June, July, August, September) for three Piacenzian interglacials (MIS G17, K1, KM3) minus the MIS KM5c and the far right column MIS KM5c minus the pre-industrial simulation showing (a) Latent heat (Wm^{-2}), (b) Salinity (PSU), (c) run off (mm day^{-1}), (d) convective rainfall (mm day^{-1}), (e) large scale rainfall (mm day^{-1}) and (f) mixed layer depth (m).